RICE UNIVERSITY

Final State Interactions in the $^{9}Be + p \longrightarrow d + 2\alpha$ Reaction

by

Sidney Thomas Emerson

A THESIS SUBMITTED
IN PARTIAL FULFILLMENT OF THE
REQUIREMENTS FOR THE DEGREE OF
DOCTOR OF PHILOSOPHY

Thesis Director's signature:

Houston, Texas
June 1968

TABLE OF CONTENTS

		Page
I.	INTRODUCTION----------	1
II.	EXPERIMENTAL APPARATUS AND PROCEDURES-----	7
	A. The Scattering Chamber----------	7
	B. Targets----------	9
	C. Electronics----------	10
	D. Calibration and Data Reduction Techniques----------	13
	E. Cross-Section Calculations----------	20
III.	THEORY----------	22
	A. Reaction Mechanisms----------	22
	B. Kinematics for Three-Body Break-Up----	23
	C. Kinematics for Sequential Break-Up----	25
	D. Effect of the Available Phase-Space---	26
	E. The Cross-Sections for Sequential Break-Up----------	29
	F. Density of States Functions----------	34
IV.	EXPERIMENTAL DATA----------	37
V.	RESULTS AND CONCLUSIONS----------	40
	APPENDICES----------	44
	A. Kinematics for Three-Body Decay-------	44
	B. Kinematics for Sequential Decay-------	46
	C. Density of States Calculations--------	49
	D. Angular Correlation Factors----------	52
	REFERENCES----------	55
	ACKNOWLEDGEMENTS----------	59

I. INTRODUCTION

Few-nucleon systems have been the object of many intensive investigations in recent years. The resurgence of interest in this field by both theorists and experimentalists has been sparked in part by the development of new technologies which permit the investigation of many-body final states in greater detail than ever before. The development of multi-parameter pulse-height analyzers, particle detectors of high resolution, time-of-flight measuring techniques, and in particular, the on-line digital computer, have made possible many previously impossible experiments. Many of these experiments have been aimed at improving our understanding of nuclear reactions involving three particles in the final state. An understanding of these three-body reactions is of fundamental importance when various models of the nucleus are considered. If these reactions proceed sequentially via a pair of two-body disintegrations, then a two-body cluster model of the nucleus would seem appropriate[1)]. A significant contribution due to simultaneous three-particle disintegration however, would necessitate the inclusion of clusters of higher order.

The reaction $^{9}Be + p \rightarrow d + 2\alpha$ has been studied by a number of authors. Blieden, et al.[2] measured elastic and inelastic cross sections from 3.5 MeV to 12.5 MeV bombarding energy. Similar measurements have been made by Morita, et al.[3] from 1 MeV to 4.6 MeV, and by Ishiwari[4] from 6.1 MeV to 7.3 MeV. Laugier, et al.[5] measured cross sections, and deduced levels and widths of $^{6}Li^{*}$ and $^{8}Be^{*}$, for bombarding energies of 7.0, 8.0, and 9.0 MeV. Beckner, Jones, and Phillips[6] studied the energy spectrum of deuterons emitted at 180° to the incident beam at a bombarding energy of 5.205 MeV. A low-energy anomaly was observed in this spectrum in the region of $E_{ex} = 0.75$ MeV, with a yield in this region of approximately 1% of the intensity of the ^{8}Be ground state yield. This anomaly has also been observed by Hay, et al.[7], and has not been accounted for by any known states of ^{8}Be or ^{6}Li.

The great disadvantage of this type of experiment is that, while the energy and momentum of one of the final state particles is determined, nothing is known of the way in which the remaining momentum is shared by the other two particles. Such an experiment integrates over all possible recoil states, and it is difficult to obtain detailed information about reaction mechanisms from such an experiment.

A complete specification of a three-body final state in which the masses of the three particles are known, requires the knowledge of nine scalar variables, i.e. the three components of momentum for each particle. The conservation of energy, and of the three components of linear momentum may be used to eliminate four of these variables. Thus measurement of the directions of the momentum vectors of two of the particles (four scalar variables) plus the kinetic energy of one of them should be sufficient. However, since the energy conservation equation is quadratic, it is necessary to measure both kinetic energies in order to determine the final state without ambiguity.

In the case of three identical particles in the final state, the conservation laws restrict the observed coincidences to a calculable locus in the E_1-E_2 plane. (See Appendix A.) The distribution of events along this locus provides a sensitive measurement of the mechanism of the reaction. If the reaction proceeds via a direct three-particle disintegration, one would expect the distribution of events along the locus to be proportional to the volume of phase space available to the particles at that point on the locus. If however, the reaction proceeds sequentially via a pair of two-body disintegrations, one would expect to observe peaking in the distribution corresponding to the

formation of metastable states in the intermediate nucleus.

If the three particles in the final state are not identical, not one but several loci will be observed if the detectors are sensitive to all particles and cannot distinguish the particle type. If, for example, all three particles are charged particles observed with ordinary solid state detectors, and no two particles are identical, one would observe six loci, corresponding to the six types of two-particle coincidences.

In the case of the reaction $^{9}Be + p \rightarrow d + 2\alpha$, three loci are observed, corresponding to d-alpha, alpha-d, and alpha-alpha coincidences respectively. These loci are not, in general, well separated in energy, and it is very difficult to obtain spectral information from a simple coincidence experiment which does not involve particle identification. Further, a particle identification system suitable for this study must have a very broad dynamic range, since the particles exhibit a broad continuum of energies.

This particle identification has been accomplished by measuring the angles of emission and kinetic energies of two particles detected in coincidence, together with the time-of-flight of one of them. If the energy, E, and the time-of-flight, t, of a particle are measured simultaneously, then the product Et^2 is proportional to the particle mass. In

order to make this measurement, one silicon surface barrier detector was situated very near the target, with another a good distance away. Three-parameter data were taken, recording the energies E_1 and E_2 of particles detected in coincidence, together with the time-of-flight difference (t_1-t_2). These data were then edited by digital computer into three parameter data of the form $(E_1,E_2,E_1t_1^2)$, where the computer has corrected the measured time (t_1-t_2) for the time-of-flight of the particle detected in the near counter, as well as for the errors in the timing measurement (walk) caused by varying pulse size in the detectors, and has formulated the product $E_1t_1^2$ for each coincident event. Two-dimensional spectra were then extracted, requiring that the particle detected in detector 1 be a deuteron (or alternatively, an alpha particle). In the case of the d-alpha locus, this technique provided a complete separation of the kinematic locus. The alpha-d and alpha-alpha loci could not, in general, be separated over the entire kinematic range, but did not exhibit large regions of overlap. In addition to providing the necessary particle identification, this technique provided a significant reduction in the background of accidental coincidences, permitting the use of much higher beam currents than would normally be used. Com-

plete details of the particle identification technique are contained in reference 8.

In this thesis, the following aspects of three-body decay will be discussed:

a) An experimental study of the $^{9}Be + p \rightarrow d + 2\alpha$ reaction, in which a complete determination of the kinematics of the final state is made.

b) An analysis of the data in terms of sequential decay and the density of states of the intermediate nuclear systems.

c) A discussion of knowledge gained from this type of experiment, and an indication of how similar experiments may be used as a spectroscopic tool to study particle unstable states in greater detail.

II. EXPERIMENTAL APPARATUS AND PROCEDURES

A. The Scattering Chamber

The experiment was performed using the 9.0 MeV proton beam from the Rice University 12 MeV tandem Van de Graaff accelerator. The scattering chamber was a brass cylinder of 30.5 cm inside diameter and 10.16 cm high, and is shown schematically in figure 1. The beam was collimated by four circular apertures in tantalum discs distributed over a distance of 43 cm. As the beam approached the target it passed through apertures of 3.18mm, 2.38mm, 2.38mm, and 3.18mm respectively. The final 3.18mm aperture was located 5.1 cm from the target center. A quartz and gunsight assembly immediately in front of the beam collimator, and a quartz at the chamber exit facilitated chamber alignment. In addition, a quartz could be inserted in the target holder to assure that the beam struck the target center. The target could be rotated about a vertical axis from outside the chamber. A Faraday cup employing permanent-magnet electron suppression was located at the rear of the chamber, and was used to monitor and integrate the target current.

Three silicon surface barrier detectors were used in the experiment--two for the coincidence measurement, and the third to monitor protons elastically scattered from ^{9}Be.

Figure 1. Schematic drawing of the reaction chamber showing the near and far counters, monitor counter, beam collimator, and target assemblies.

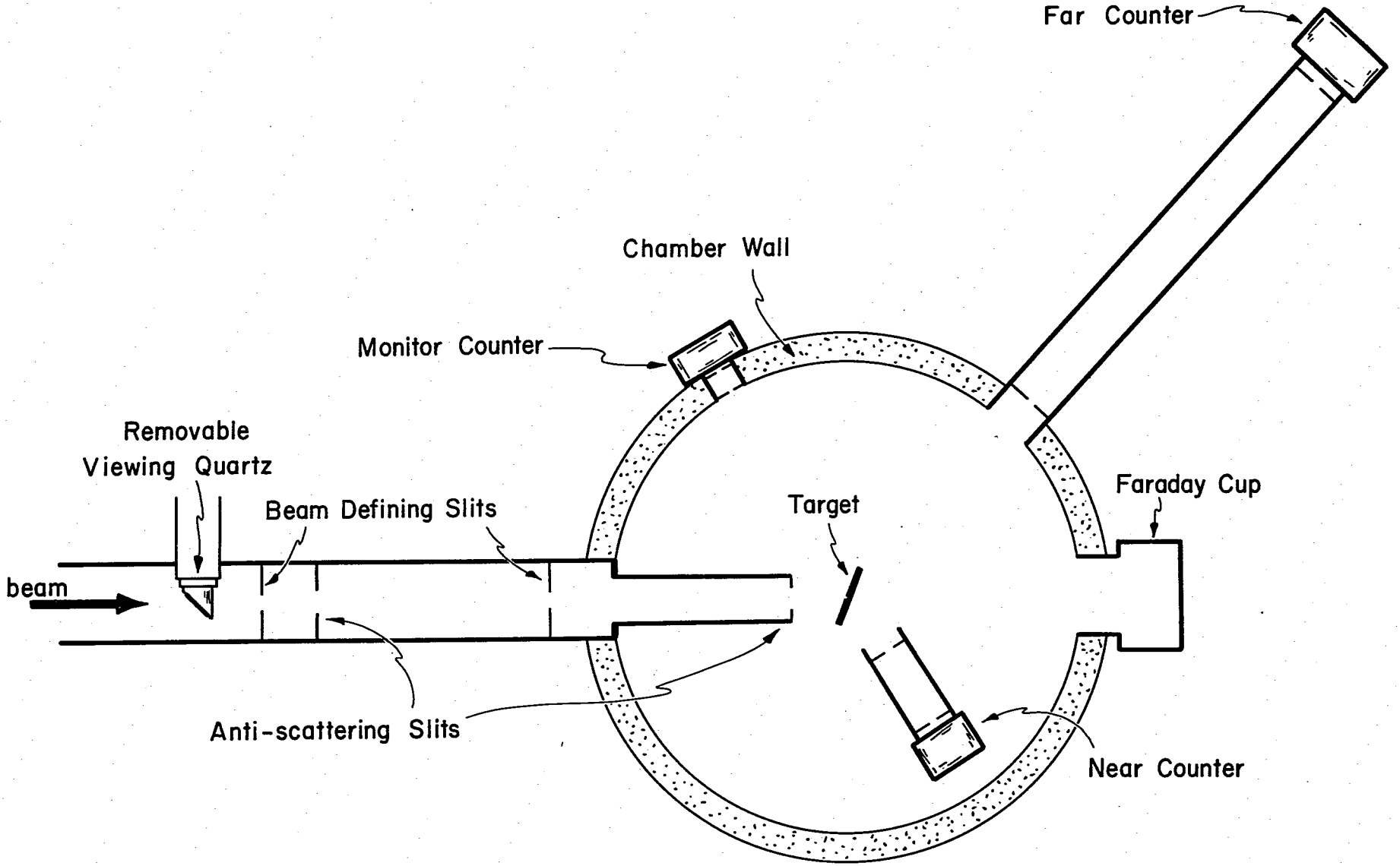
Far Counter
Chamber Wall
Monitor Counter
Removable
Viewing Quartz
Beam Defining Slits
Target
Faraday Cup
beam
Anti-scattering Slits
Near Counter

The "near" counter was mounted on the chamber lid a distance of 5.3 cm from the target center, and could be moved to any angle from 20° to 160° to the incident beam. The slit telescope associated with this counter consisted of two 3.18 mm circular apertures in tantalum discs located 5.1 cm and 2.56 cm from the target center respectively. The "far" counter could be affixed to any one of fifteen ports in the chamber wall, located at 10° intervals from 20° to 160° to the incident beam. The surface of this counter was 72 cm from the target center. The slit telescope associated with this counter consisted of a 13.5 mm aperture located 71 cm from the target center and a 3.8 mm aperture located 17.8 cm from the target center. These two counters subtended solid angles of 3.07×10^{-3} sr. and 2.83×10^{-4} sr. respectively. The monitor counter could also be affixed to any one of the fifteen side ports in the chamber, and was held a distance of 18.4 cm from the target center. The slit system for the monitor counter consisted of two 3.18 mm diameter circular apertures in tantalum discs located 15.2 cm and 17.75 cm from the target center respectively. This counter subtended a solid angle of 2.33×10^{-4} sr.

Because of the necessity of making very fast timing measurements, the solid state detectors were selected with great care. These were silicon surface barrier detectors of

1,000 micron depletion depth, and were selected so as to minimize the charge collection time. The "near" counter was a 3,000 ohm-cm device operated at 900 volts bias, and had a surface area of 25 mm^2. The "far" counter was a 200 mm^2 device, of 9,500 ohm-cm resistivity, and was operated at 450 volts bias. These detectors had gold dead layers of 0.3 mg/cm^2 thickness.

B. Targets

Self-supporting ^9Be foils were prepared by evaporating beryllium metal under high vacuum onto clean glass slides coated with tepol, a commercial detergent. A tungsten boat was used to heat the beryllium for the evaporation. The foils were then floated off the glass in a warm water bath and deposited on the target holders. Great care was taken to avoid personal contact with the beryllium metal or inhalation of the vapor, due to the poisonous properties of the element. The targets used in the experiment were approximately 50 KeV thick to the incident protons. Principal impurities were carbon and oxygen. The target was insulated from ground and held at several hundred volts positive bias to prevent low energy electrons from reaching the detectors.

C. Electronics

The signals from the detectors were processed by the circuits shown in figure 2. An overall timing resolution near 1 nanosecond was necessary to effect the desired mass identification over the full energy range. Such time resolution is not possible at the current state of the art using double delay line clipped amplifiers and zero cross-over timing. Therefore it was necessary to use a timing signal derived from the leading edge of the pulse. The inherent timing error in this type of time pick-off due to varying pulse size (walk) was greatly reduced by the technique described in the next section. Ortec Model 260 time pick-off units were used. However, the current pulses from the detectors were too small to trigger the time pick-off units directly for particle energies below about 3 MeV. This difficulty was overcome by inserting the time pick-off pulse transformer in series with the cathode of the third cascode amplifier stage of the Tennelec Model 100 charge sensitive preamplifier. This provided sufficient gain to lower the time pick-off threshold to about 0.5 MeV. The inductance of the time pick-off pulse transformer was sufficiently small to have negligible effect on the output pulses of the charge sensitive preamplifier. The time pick-

Figure 2. Block diagram of the electronic circuit used in the Et^2 measurements.

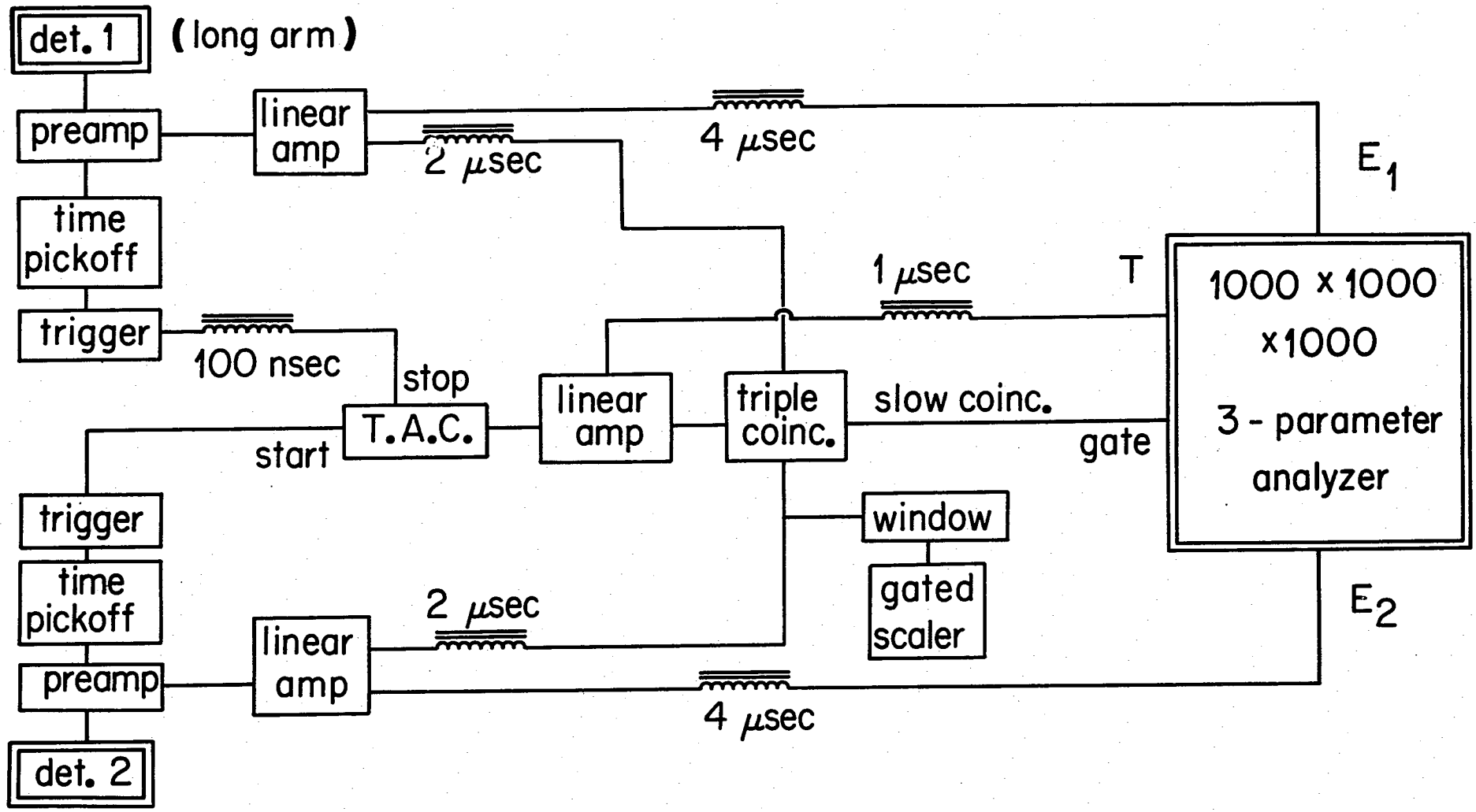
det. 1
(long arm)
preamp
linear amp
4 μsec
2 μsec
E1
time pickoff
trigger
1 μsec
T
1000 x 1000 x1000
3 - parameter analyzer
100 nsec
stop
linear amp
triple coinc.
slow coinc.
T.A.C.
start
gate
trigger
window
time pickoff
gated scaler
2 μsec
linear amp
E2
preamp
4 μsec
det. 2

off units provided output pulses of -0.5 volts, with a rise time of less than 2 nanoseconds and a width of 10 nanoseconds. These signals were fed into EG&G Model TR104 fast trigger modules, which were used to shape the pulses appropriately for the time-to-amplitude converter. The EG&G Model TH200 time-to-amplitude converter was used in the experiment, and was operated on the 0 to 300 nanosecond scale. This device had a time resolution of better than 0.1 nanoseconds, and an integral linearity of better than 0.2% in the upper 90% of its range. A constant delay of 100 nanoseconds was inserted in the stop signal to insure that all pulses of interest were in the upper two-thirds of the TAC range.

The signals from the two Tennelec Model 100 preamplifiers were then fed to Ortec Model 410 linear amplifiers operating in a double delay line clipped mode. The TAC signal was amplified by a Tennelec Model TC200 linear amplifier in an RC shaped mode. The bipolar outputs of the Ortec amplifiers (with appropriate delays inserted) were then placed in triple slow coincidence (1 microsecond) in a Cosmic Model 900 coincidence circuit. This provided a gating signal for the Rice 3-parameter 1,000 x 1,000 x 1,000 channel computer analyzer[9]. In addition, it provided added flexibility in several ways. First, free spectra could be

taken from the detectors merely by changing the analyzer program from multi-parameter to single-parameter data capture and relaxing the coincidence gating requirement. Second, windows could be set to avoid recording accidental coincidences which lay outside the region of experimental interest. Third, a slow bias was set slightly above the fast bias of the time-pick-off units to avoid distortion of the data due to slight drift which might be present in the fast circuits, and to reduce background due to noise in the time-pick-off circuits.

The signals from the monitor counter (which was set at 120° for these experiments) were fed into a Tennelec Model 100 charge sensitive preamplifier, and an Ortec Model 410 linear amplifier operating in a double delay line clipped mode. The amplified signals were then fed into a Cosmic Model 900 single channel analyzer set about the peak of protons elastically scattered from ^{9}Be. Pulses inside this window were recorded in a scaler which was automatically gated off during analyzer dead time. This provided an accurate measurement of the ratio of the elastic and inelastic scattering cross-sections for the d + 2α channel.

The Rice University three-parameter computer analyzer was used to record the three-parameter data. The device consisted of two Astro-Data Model 3000 analog-to-digital

converters, each with 1000 channels output. These were operated in a multiplexed configuration to provide the three-parameter data capture capability. Digital interfacing provided direct access to a magnetic core data buffer in the IBM 1401 on-line computer. Two hundred three-parameter events were required to fill the data buffer. When the buffer was filled, the data were automatically written to magnetic tape, a 25x25 channel two-parameter coarse sort of the data was up-dated, the buffer was cleared, and the capture resumed. Additional details of the computer-analyzer may be found in reference 9.

D. Calibration and Data Reduction Techniques.

The task of converting the data from the capture format on magnetic tape into sets of usable two-dimensional spectra in which the mass of one particle was known required careful and accurate calibration of all experimental parameters. Particular care was required to obtain an accurate calibration along the timing axis, since this provided the key to the mass identification scheme. The slope of the time channel was obtained by starting the time-to-amplitude converter with a 10 nanosecond width logic pulse, and stopping it with the same pulse delayed by a known amount. By repeating this procedure through several such delays, an

accurate linearity check of the timing circuitry was made. The linearity of the circuitry associated with the two energy axes was checked using a BNC Model RP-1 tail pulse generator. The linearity of all these circuits was better than 1%. Absolute calibrations of the two energy axes were obtained by programming the computer-analyzer in a single parameter data capture configuration, and relaxing the coincidence gating requirements, thus taking free spectra from each detector. These free spectra were taken for several angles of the detectors, and generally were checked periodically during a long data capture run.

An absolute calibration of the timing axis was obtained by scattering protons from a thin deuterated polyethylene foil. This reaction produces knocked out deuterons at 30° to the incident beam which are coincident with elastically scattered protons at 90°. A series of such runs was made, varying the proton bombarding energy from 2.0 MeV to 11.0 MeV in steps of 1.0 MeV, detecting the d-p coincidences, and measuring the three parameters E_1, E_2, and t_1-t_2, where E_i is the energy of the particle in detector i, and t_i is its measured time-of-flight from the target to the detector. The two counters were then physically reversed (the 30° counter placed at 90° and vice versa) and the measurements repeated. The calculated time-of-flight

difference was then plotted vs. the measured time-of-flight difference. A typical result is shown in figure 3a. The result is not a single straight line, but two lines, with slightly different slopes. This is a consequence of the leading edge timing technique, which has an inherent timing error (walk) due to the finite time required for the pulse to rise to the discrimination level. Since a fixed voltage discrimination level is set to obtain a timing trigger pulse, a time walk will be observed which is, to a first approximation, inversely proportional to the pulse height (and hence, to the energy of the incident particle). Since the two pulse heights are also measured, it is possible to correct each measured time difference for the error due to the inherent walk of the leading edge discriminators. Figure 3b shows the same data as figure 3a after a linear correction for discriminator errors has been applied. The result is a single straight line of the proper slope. The point at which this line intersects the horizontal axis gives an accurate measure of the total electronic delay in the circuit.

A simple least-squares fitting program was written which calculated the best correction constants and the timing intercept, from the p + d elastic timing data and the slope of the time channel. These constants were then used by the

Figure 3. Two-body calibration data for time-of-flight measurements for proton bombardment of a deuterated polyethylene foil with elastically scattered protons and deuterons detected in coincidence. Figure 3a (upper graph) shows the calculated time-of-flight difference for p-d and d-p coincidences, without correcting for the discriminator timing error. Figure 3b (lower graph) shows the same data with the timing correction.

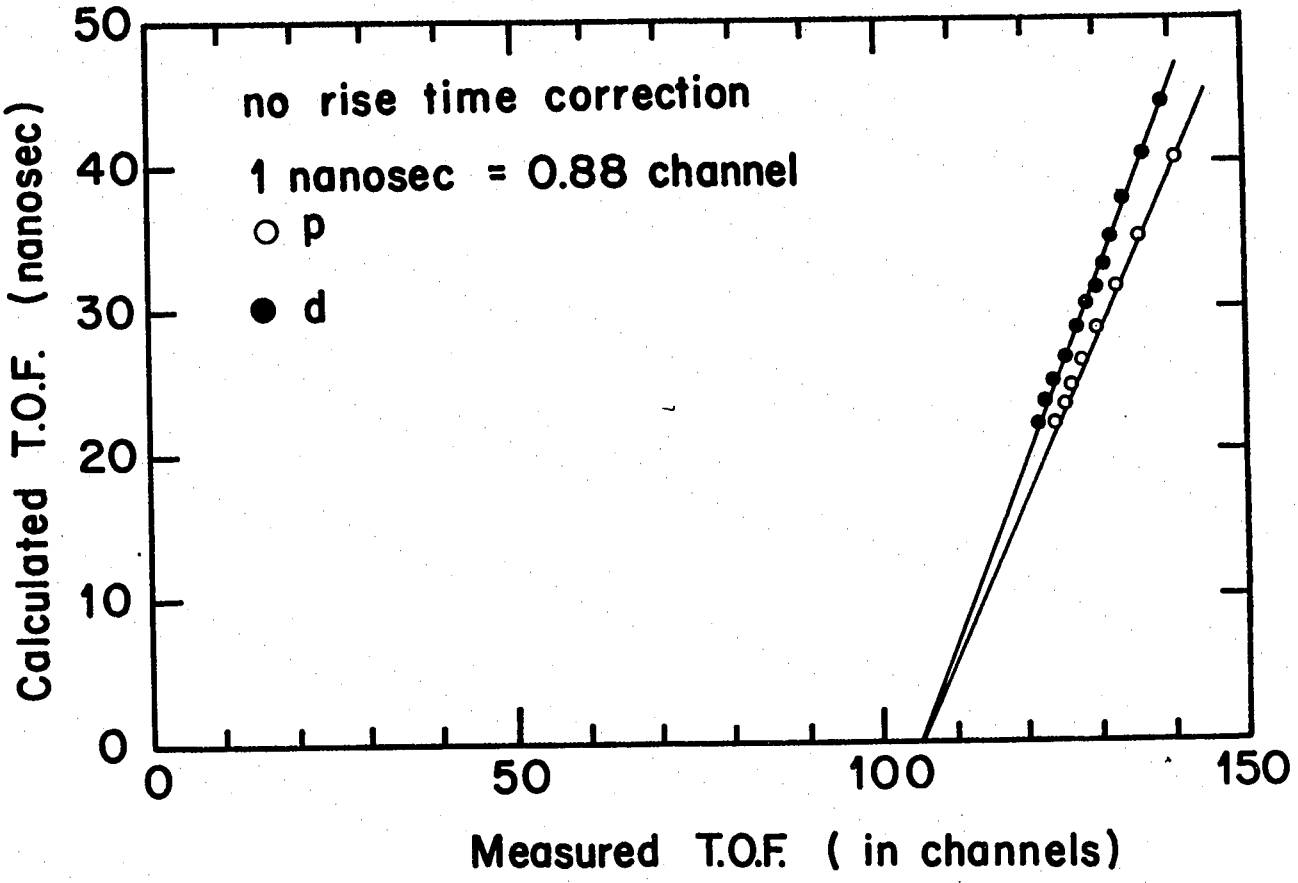
no rise time correction
1 nanosec = 0.88 channel
○ p
● d
Calculated T.O.F. (nanosec)
Measured T.O.F. (in channels)
0
10
20
30
40
50
0
50
100
150

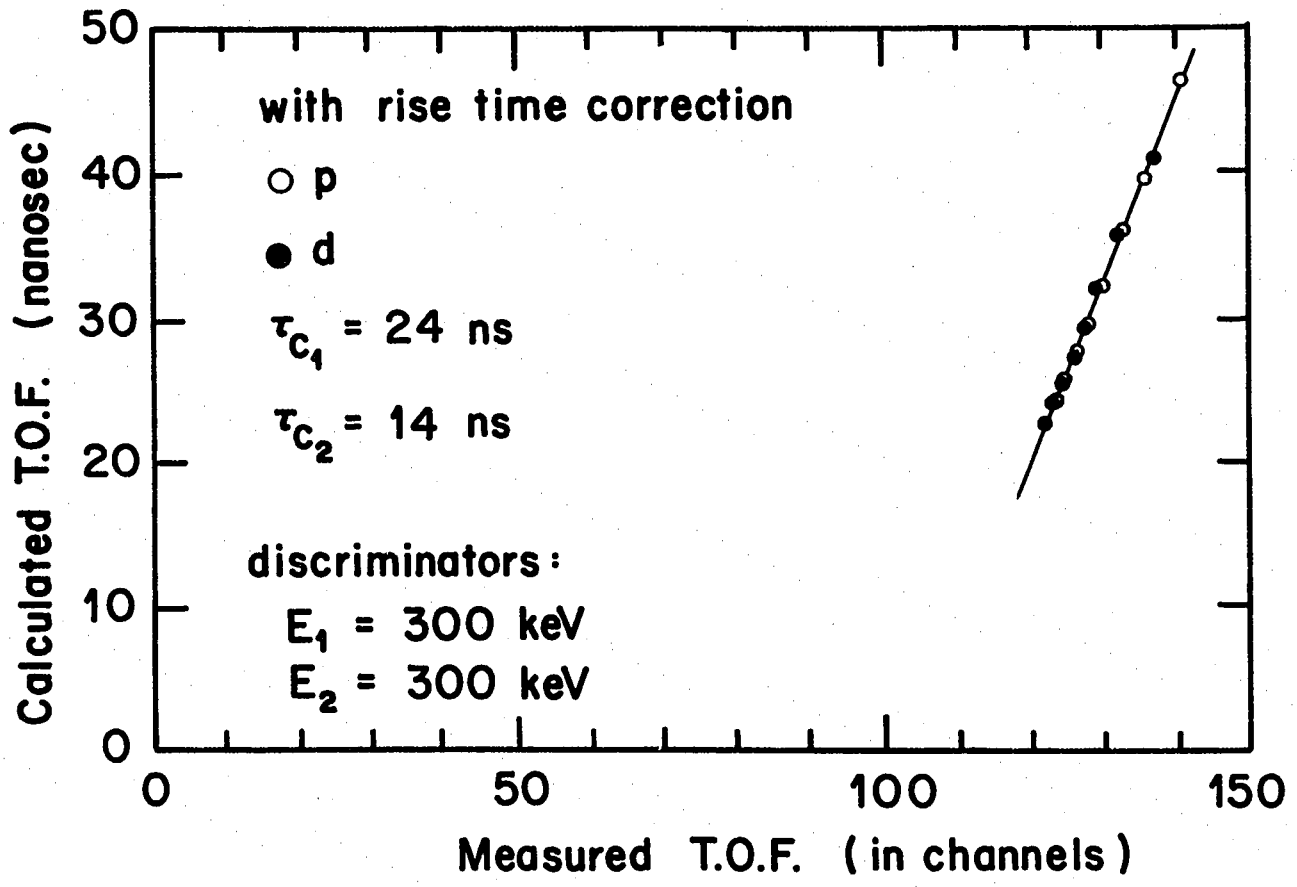
with rise time correction
○ p
● d
τ_{C_1} = 24 ns
τ_{C_2} = 14 ns
discriminators:
E_1 = 300 keV
E_2 = 300 keV
Calculated T.O.F. (nanosec)
Measured T.O.F. (in channels)
0
10
20
30
40
50
0
50
100
150

Et^2 edit program described below.

The quantity which we wish to determine for each coincident event is the product of the energy E_1 of the particle in detector 1, and the square of its time-of-flight t_1, $(E_1 t_1^2)$. However we have measured not t_1, but $t_1 - t_2$, where t_2 is the time-of-flight of the particle in detector 2 (near detector). If the particle in detector 2 is a very energetic light particle, then its time-of-flight will be small compared to the time-of-flight of the particle in the far detector. However, for low energy start particles one should not ignore the time-of-flight of the start particle. Since we do not know the mass of the start particle, we cannot calculate its time-of-flight exactly. However, we have measured its energy, and we know that for the reaction under study, the start particle must be either an alpha particle or a deuteron. Suppose that we assume the start particle to be an alpha particle. This assumption should be correct for approximately 2/3 of the coincident events, since there are two alphas and a deuteron in the final state of the reaction under study. If, however, the start particle were not an alpha particle, but a deuteron, our incorrect assumption will cause us to calculate a time-of-flight for this deuteron which is too large by a factor of $\sqrt{2}$. If this time is added to the measured time, the result squared

and multiplied by E_1, the resulting value of $E_1 t_1^2$ will also be too large. But for the reaction under study, if the start particle were a deuteron, the stop particle was necessarily an alpha particle, and the calculated value of $E_1 t_1^2$ for this alpha was in error in the direction of greater separation of deuterons from alphas. The effect of the error in the mass assumption for the start particle has actually helped, rather than hindered the separation of deuterons from alphas.

An Et^2 data edit program was written for the IBM 1401 computer which converted the data from the capture format $(E_1, E_2, t_1 - t_2)$ into the form:

$$E_1, E_2, \frac{E_1 (T - T_o + C_1/\sqrt{E_2} - C_2/E_1 + C_3/E_2)^2}{N}$$

where T is the experimentally measured time, T_o is the constant delay in the electronic circuit, C_1 corrects for the time-of-flight of the start particle (assuming it to be an alpha particle), C_2 and C_3 correct for the time walk of the discriminators, and N is a normalization constant. This function very closely approximates the mass invariant quantity $E_1 t_1^2$.

A three-parameter to two-parameter data edit program was then used to edit these data in the Et^2 format to a

two-parameter format, with limits on the third parameter. The data reduction technique was as follows: First the three-parameter data from the data capture program were edited to three-parameter data in the Et^2 format. Second, a two-dimensional spectrum of $E_1 t_1^2$ vs. E_1 was obtained, using the three-parameter to two-parameter edit program. A typical spectrum of this type is shown in figure 4, and its projection on the $E_1 t_1^2$ axis is shown in figure 5. Bands of counts occur corresponding to deuterons and alpha particles from the three-body reaction. In addition, low energy protons are observed from the four-body reaction $^9Be + p \rightarrow p + n + 2\alpha$. The appropriate limits on the Et^2 parameter were then chosen, and the three-parameter to two-parameter edit program was used to extract energy-energy spectra, requiring alternately that particle 1 be an alpha particle or a deuteron. The calculated kinematics curves were then plotted on the spectra, and the intensities examined.

Aside from providing the necessary particle identification, the Et^2 technique provided a significant reduction in the background due to random coincidences. These random coincidences, for continuum particles whose energy is more or less continuously dispersed over energy bands extending uniformly to the maximum energies $E_{1\ max}$ and $E_{2\ max}$ and with

Figure 4. A typical spectrum of $E_1 t_1^2$ *vs.* E_1. Note bands of intensity corresponding to deuterons and alpha particles.

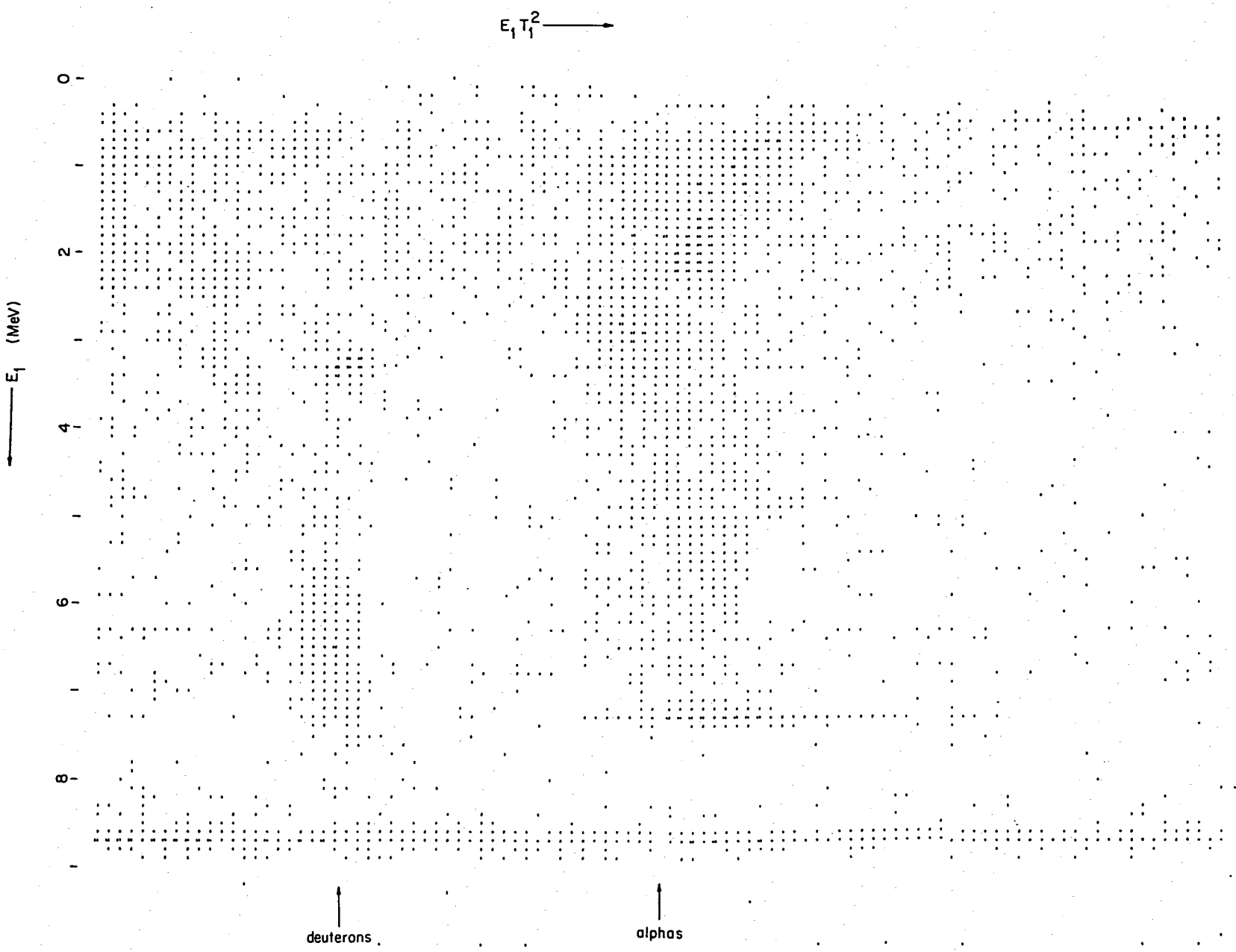
$E_1 T_1^2$
E_1 (MeV)
0
2
4
6
8
deuterons
alphas

Figure 5. Projection of the data of figure 4 on the $E_1 t_1^2$ axis.

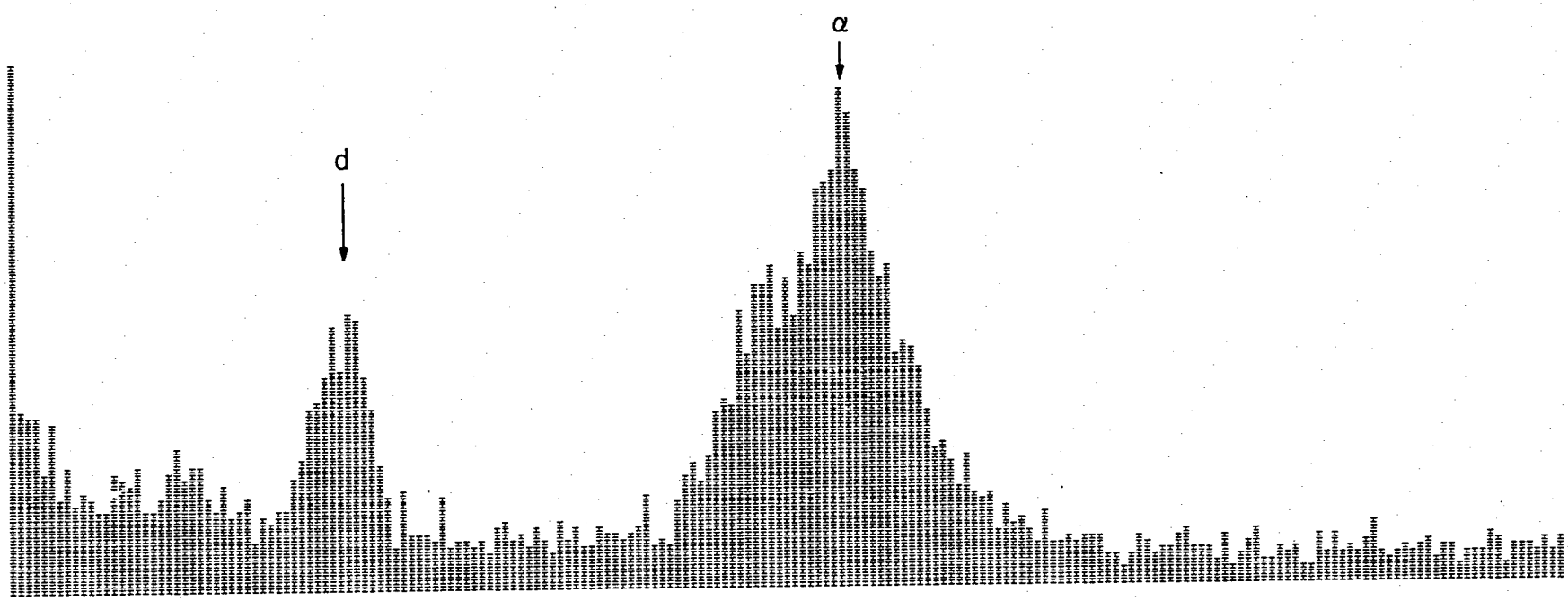
Projection of Et^2 Spectrum
α
d

time-of-flight differences extending uniformly to the maximum time-of-flight observable, have the property that they populate equal increments of Et^2 more or less equally. Since the data were digitized so that the three parameters were each recorded in 1,000 channels, the total dynamic range for random coincidences, D_R, of Et^2 is 10^9 $(\text{channels})^3$. However, for true coincidences, $Et^2 = 1/2m_A d^2$, where $m_A = Am_{proton}$, and d is the flight distance, and this quantity has a much smaller dynamic range, D_T. For example, if a distance d = 70 cm is chosen, E = 10 MeV, and T = 300 nsec, then $D_R = 9 \times 10^5$ MeV-nsec^2, while $D_T = 2550A$ MeV-nsec^2. Thus the background improvement factor is $D_R/D_T = 350/A$.

Figures 6, 7, and 8 illustrate the effectiveness of the particle identification technique. Figure 6 shows a typical energy-energy coincidence spectrum without particle identification, taken with a coincidence resolution τ_C = 30 nsec. Figures 7 and 8 show data taken under identical conditions except that counter 1 has been moved from 5.7 cm to 71 cm from the target, its slit telescope has been changed so as to maintain the same solid angle, and the Et^2 technique with a 300 nsec time window has been used to identify the particle in detector 1 as either a deuteron (fig. 7) or an alpha particle (fig. 8). It is noted that very good mass

Figure 6. Coincidence spectrum for $^{9}Be + p$ without particle identification. The two detectors have bands of overlapping (d-α), (α-d), and (α-α) coincidences as well as a background of accidental coincidences. $\theta_1 = 30°$, $\theta_2 = 100°$, $E_p = 9.0$ MeV.

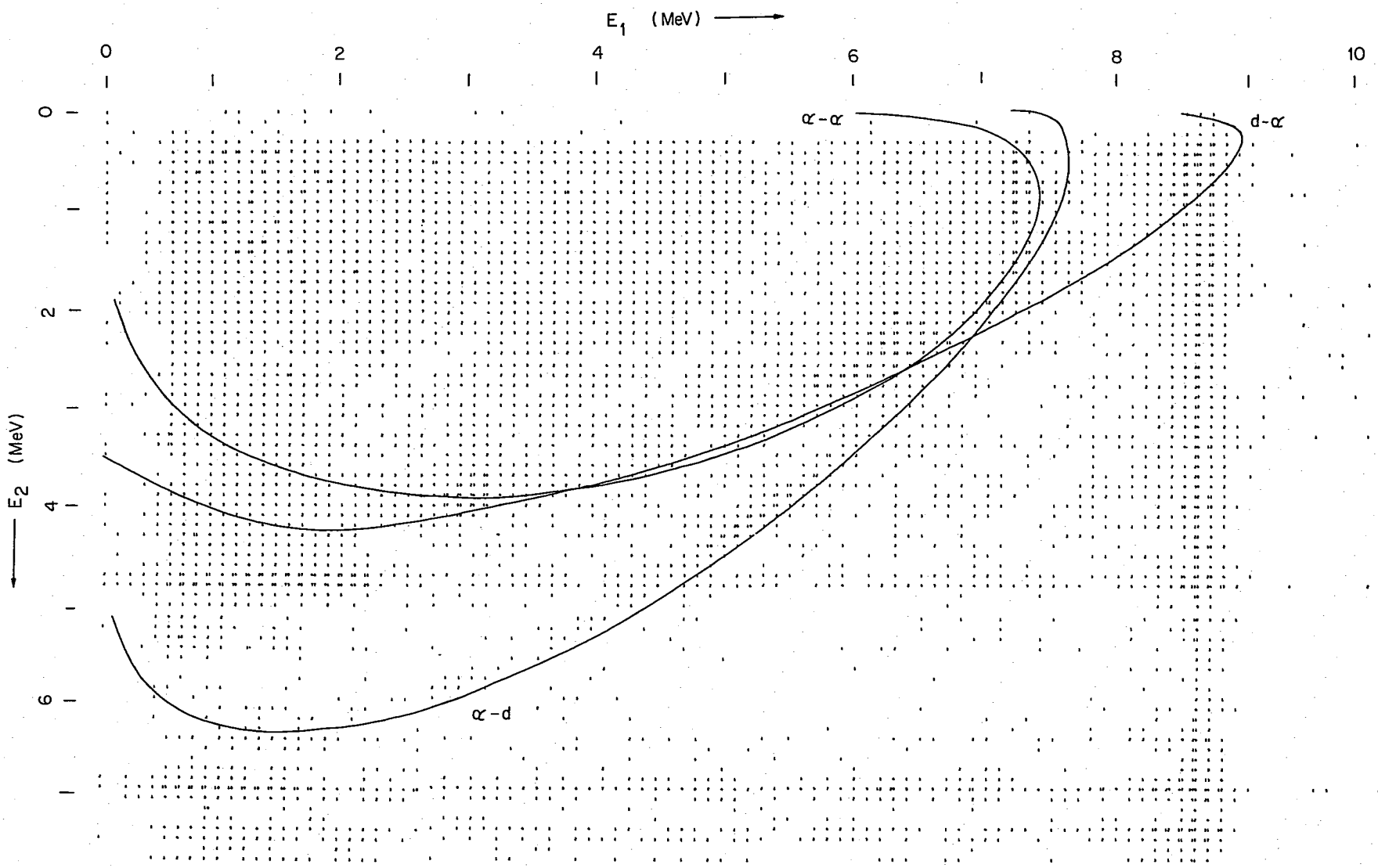
E1 (MeV)
0
2
4
6
8
10
E2 (MeV)
0
2
4
6
α-α
d-α
α-d

Figure 7. Data taken under identical conditions to that of figure 6, but with the Et^2 particle identification system used to identify particle 1 as a deuteron.

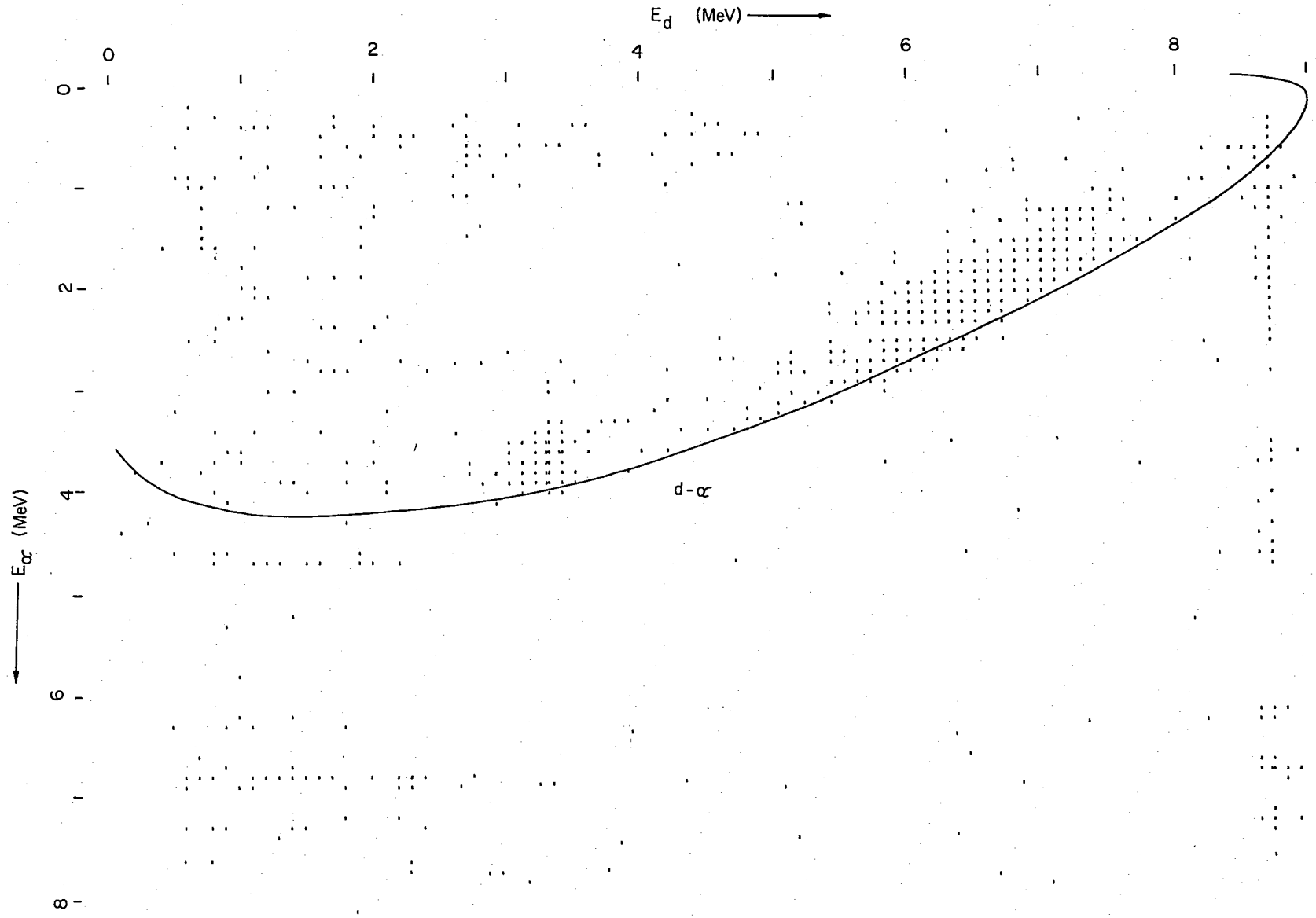
E_d (MeV)
0
2
4
6
8
E_α (MeV)
0
2
4
6
8
d-α

Figure 8. The same data run as in figure 7, but using the Et^2 particle identification technique to require that particle 1 be an alpha particle. In addition to the (α-d) and (α-α) three-body loci, a background of alpha particles from the four-body reaction $^{9}Be + p \rightarrow p + n + 2\alpha$ is also evident.

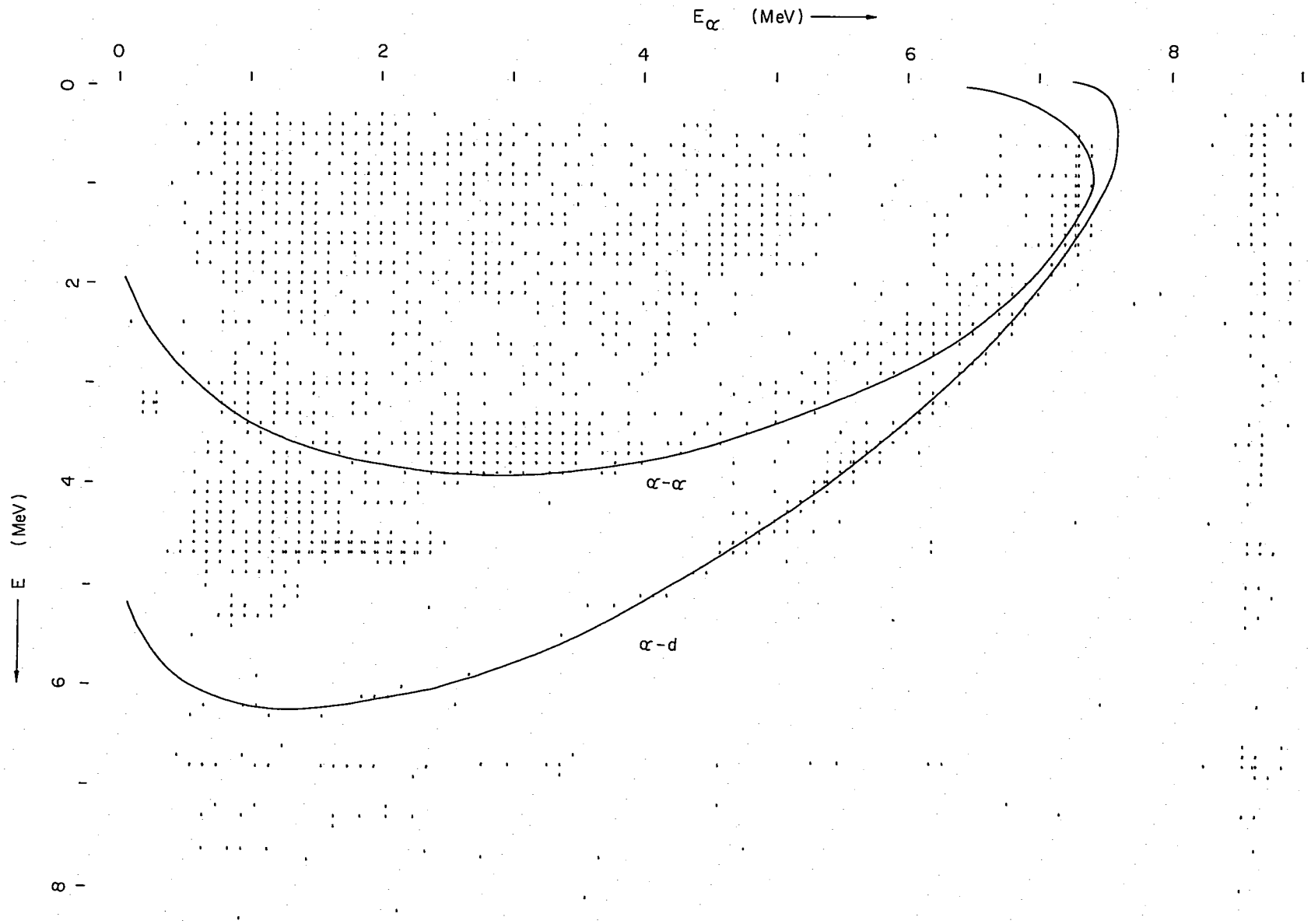
E_α (MeV) ⟶
0
2
4
6
8
E (MeV)
α-α
α-d

separation has been attained with very low accidental background. The alpha particle spectrum (fig. 8) shows a continuum of low energy alpha particles from the four-body reaction $^{9}Be + p \rightarrow p + n + 2\alpha$. Comparison of the accidental backgrounds of figures 6, 7, and 8 shows that the Et^{2} particle identification has afforded a background reduction of more than a factor of 15.

E. Cross-Section Calculations

For all of the experimental data presented, the differential cross-sections were measured in ratio to the elastic scattering cross-section of protons from ^{9}Be at a fixed monitor counter angle. This monitor counter angle was chosen so as to assure separation of protons elastically scattered from ^{9}Be from the elastic protons from ^{12}C, a principal target impurity. The laboratory angle selected for the monitor counter was $\theta_M = 120°$. The differential cross-section for the three-body decay was then calculated using the relation:

$$\frac{d^3\sigma(T_1, \Omega_1, \Omega_2)}{dT_1\, d\Omega_1\, d\Omega_2} = \frac{N_{12}(\theta_1, \theta_2)\, \frac{d\sigma_{elas}(\theta_M)}{d\Omega_M}\, \Delta\Omega_M}{N_M(\theta_M)\, \Delta T_1\, \Delta\Omega_1\, \Delta\Omega_2}$$

where

$N_{12}(\theta_1,\theta_2)$ = Number of counts on the three-body locus in the energy increment ΔT_1 at laboratory angles θ_1 and θ_2 and solid angles $\Delta\Omega_1$ and $\Delta\Omega_2$.

$N_M(\theta_M)$ = Number of counts in the elastic proton peak at laboratory angle θ_M and solid angle $\Delta\Omega_M$.

$\frac{d\sigma_{elas.}(\theta_M)}{d\Omega_M}$ = Differential cross-section of protons elastically scattered from ^{9}Be at laboratory angle θ_M.

The elastic scattering cross-section was taken from the data of Blieden, et al.[2] as

$$\frac{d\sigma_{elas.}(\theta_M)}{d\Omega_M} = 18 \pm 3 \text{ mb/sr.}$$

at 120° lab., and bombarding energy of 9 MeV.

III. THEORY

A. Reaction Mechanisms

Protons incident upon a ^{9}Be target could interact to produce a d + 2α final state *via* several mechanisms. One expects *a priori* that one or more of the following mechanisms will contribute:

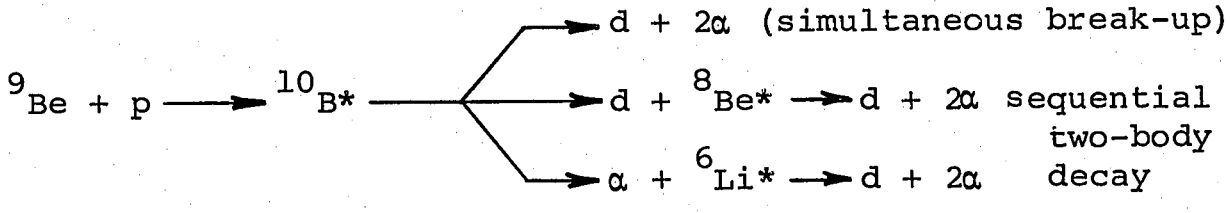

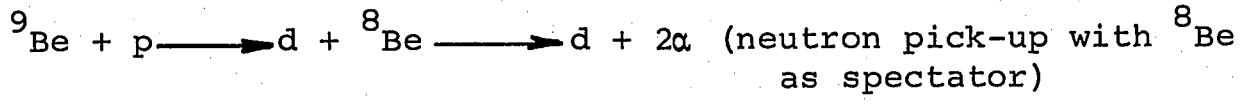

Much experimental evidence indicates that, for light nuclei and for bombarding energies below about 15 MeV, the sequential two-body decay mechanisms are dominant. (See references 10-16.) For most reactions of this type, strong resonances between pairs of particles exist, and these final state interactions contribute strongly to the yield. The matrix elements for this process are fairly well understood, primarily due to the work of Watson[17], Migdal[18], and Phillips[19].

The neutron pick-up mechanism would not be expected to contribute significantly to the coincidence yield if the ^{8}Be spectator is left in its ground state, since the alpha particles from this decay would be below the energy threshold of the detectors. If however, the ^{8}Be spectator were left in the 2.90 MeV state, or higher states, this decay could be seen in a coincidence experiment.

Jackson[20] and Niiler[21] have found evidence for direct single-nucleon knock-out in the p + d $\rightarrow$ 2p + n reaction. However, since there is no proton in the final state of the ^{9}Be + p $\rightarrow$ d + 2α reaction, this mechanism cannot contribute. Valkovic *et al.*[22] have considered the possibility of higher order mechanisms, including the effect of rescattering of the final state particles, but little experimental evidence is available concerning these higher order mechanisms.

B. Kinematics for Three-Body Break-Up

The loci in the energy-energy plane for the detection of two particles from a three-body nuclear reaction are a function only of the angles of the detectors, the energy and mass of the beam particle, the Q-value of the reaction, and the masses of the final state particles. It is possible to calculate these loci directly from the conservation of energy and linear momentum. This calculation is done in

Appendix A. There are six loci for three non-identical particles, but these degenerate to three loci if two of the particles are identical, and to one locus for three identical particles.

A convenient coordinate system for the description of the three-body final state is that used by Simpson et al.[14], and is shown in figure 9. Here θ_i is the angle between $\bar{P}_i$ (the lab momentum of particle i) and the beam axis, $\bar{P}_o$ is the momentum of the beam particle (directed along the z-axis), and ϕ_i is the angle about the beam axis measured in the x-z plane from the positive x-axis. The incident beam particle has momentum $\bar{P}_o$, mass m_o, and kinetic energy T_o. The three final state particles have masses m_1, m_2, and m_3, momenta $\bar{P}_1$, $\bar{P}_2$, and $\bar{P}_3$, and kinetic energies T_1, T_2, and T_3. In this coordinate system, the locus (in momentum space) for P_2 as a function of P_1 is given by

$$P_2 = \frac{-B \pm \sqrt{B^2-4AC}}{2A}$$

where

$$A = \frac{1}{2}\left[\frac{1}{m_3} + \frac{1}{m_2}\right]$$

$$B = \frac{1}{m_3}\left[P_1\cos\theta_1\cos\theta_2 + P_1\sin\theta_1\sin\theta_2\cos(\phi_1-\phi_2) - P_o\cos\theta_2\right]$$

$$C = \left[P_o^2\left(\frac{1}{2m_3} - \frac{1}{2m_o}\right) + P_1^2\left(\frac{1}{2m_1} + \frac{1}{2m_3}\right) - \frac{1}{m_3}[P_oP_1\cos\theta_1] - Q\right]$$

Figure 9. Diagram showing the convention adopted for measuring the detector angles. The z-axis coincides with the beam axis.

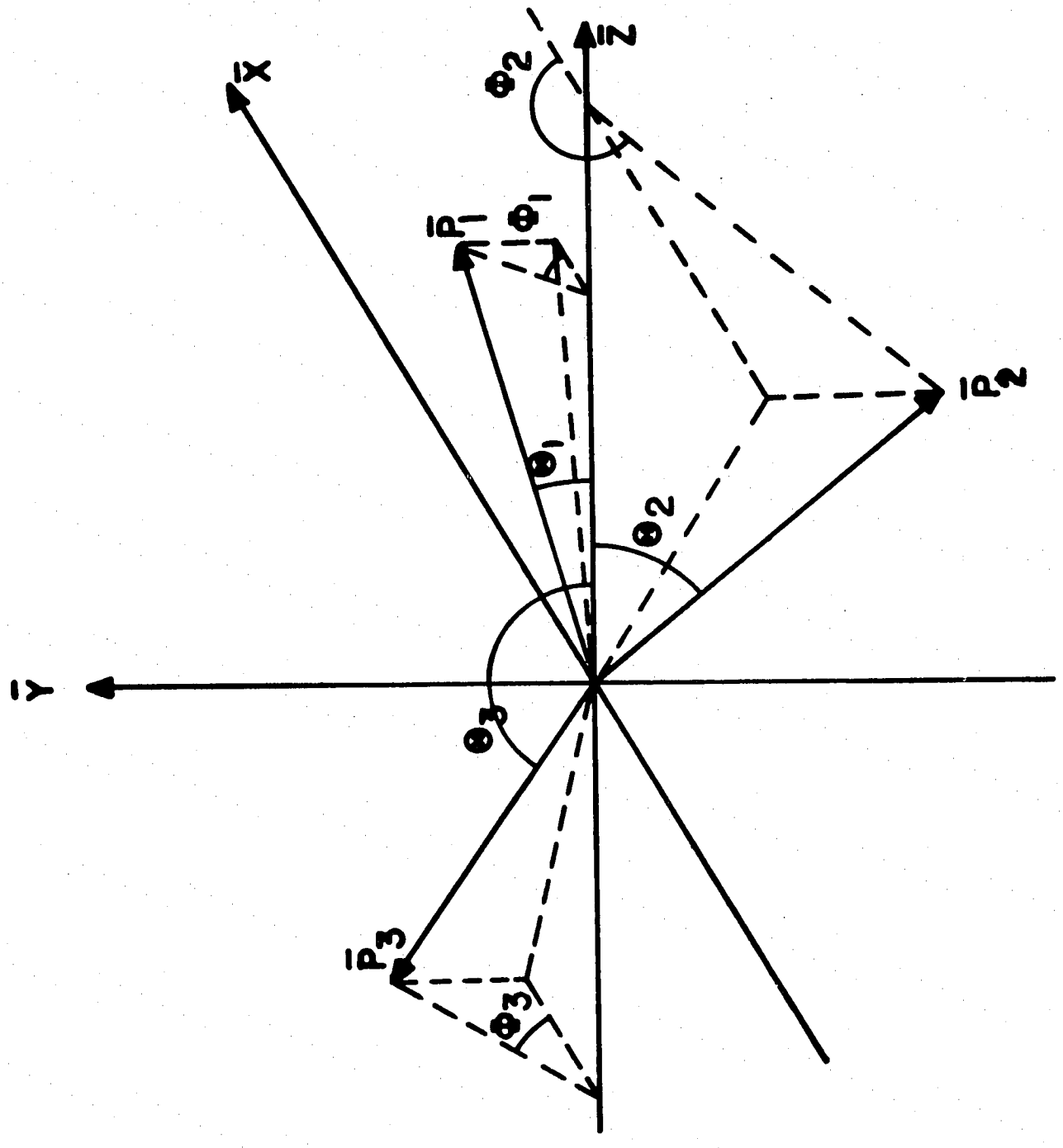
iX
iZ
iY
θ_2
$\bar{P}_1$
θ_1
$|P_2$
θ_1
θ_2
θ_3
$|P_3$
θ_3

and Q is the Q-value for the three-body break-up. Using this momentum relation, the locus for T_2 as a function of T_1 is readily calculable. The above equation represents a closed curve in momentum space, but since only particles with positive momentum (i.e. those traveling toward the detectors) will be observed in the coincidence experiment, the entire locus may not be seen.

C. Kinematics for Sequential Break-Up

There are three possible sequential two-body decay mechanisms, corresponding to particle 1, 2, or 3 being the first emitted, leaving the other two particles in an intermediate state which subsequently decays. For each point on the locus, it is possible to calculate the internal energy in this intermediate state for each of the three sequential decay mechanisms. These relations are derived in Appendix B, and the results are quoted below:

$$E_{23} = T_o + Q - T_1 - \frac{1}{2m_{23}} (P_o^2 + P_1^2 - 2P_oP_1\cos\theta_1)$$

$$E_{13}^{\pm} = T_o + Q - T_2^{\pm} - \frac{1}{2m_{13}} (P_o^2 + (P_2^{\pm})^2 - 2P_oP_2^{\pm}\cos\theta_2)$$

$$E_{12}^{\pm} = T_o + Q - \frac{P_o^2}{2m_3} + \frac{P_o}{m_3} (P_1\cos\theta_1 + P_2^{\pm}\cos\theta_2)$$

$$- \frac{1}{2}\left(\frac{1}{m_3} + \frac{1}{m_{12}}\right)\left\{P_1^2 + (P_2^{\pm})^2 + 2P_1P_2^{\pm}[\cos\theta_1\cos\theta_2 + \sin\theta_1\sin\theta_2\cos(\phi_1-\phi_2)]\right\}$$

where E_{23} is the internal energy in the (2,3) system, assuming sequential decay with particle 1 first emitted, etc. The $\pm$ signs indicate the branch of the quadratic momentum relation given in the preceding section. If a resonance exists in one intermediate system, this will produce peaking in the observed yield at the point on the locus corresponding to the resonant energy in the intermediate system.

D. Effect of the Available Phase-Space

Several authors[14,20,23,24] have considered the problem of calculating the volume of phase-space available to a three-body disintegration as observed in the laboratory reference frame. An understanding of the effect of the available phase-space is of great importance in interpreting three-body reaction data. This is particularly true since a simultaneous three-body disintegration is expected to produce a laboratory yield proportional to the available phase-space. Therefore, a brief derivation of the phase-space factor will be presented here.

Consider the probability of finding particle 1 in solid angle Ω_1 with momentum between P_1 and P_1+dP_1 when particle 2 is detected in solid angle Ω_2, assuming that this probability is proportional to the available phase-space. Due to the experimental conditions, only the case of

planar break-up will be considered. However, the argument is easily generalized for the non-planar case. Denoting $d\bar{P}_i$ by $P_i^2 dP_i d\Omega_i$, the total phase-space volume N_t may be written as

$$N_t = \int_{\bar{P}_1}\int_{\bar{P}_2}\int_{\bar{P}_3} \delta\left(E - \sum_{j=1}^{3} \frac{P_j^2}{2m_j}\right) \delta\left(\sum_{K=1}^{3} \bar{P}_K - \bar{P}_o\right) d\bar{P}_1 d\bar{P}_2 d\bar{P}_3$$

where E is the total energy of the three-body system, and the delta functions conserve energy and linear momentum.

Integrating over $\bar{P}_3$ we obtain

$$N_t = \int_{\bar{P}_1}\int_{\bar{P}_2} \delta\left(E - \frac{P_1^2}{2m_1} - \frac{P_2^2}{2m_2}\right) - \frac{(\bar{P}_o - \bar{P}_1 - \bar{P}_2)\cdot(\bar{P}_o - \bar{P}_1 - \bar{P}_2)}{2m_3} \, d\bar{P}_1 d\bar{P}_2$$

$$N_t = \int_{P_1}\int_{\Omega_1}\int_{P_2}\int_{\Omega_2} \delta\left(E - \frac{P_1^2}{2m_1} - \frac{P_2^2}{2}\left[\frac{1}{m_2} + \frac{1}{m_3}\right] + \frac{1}{m_3}\left[\bar{P}_1\cdot\bar{P}_o + \bar{P}_2\cdot\bar{P}_o - \bar{P}_1\cdot\bar{P}_2\right]\right)$$

$$\cdot P_1^2 P_2^2 \, dP_1 d\Omega_1 dP_2 d\Omega_2$$

The above delta function may be changed to a delta function of P_2 using the appropriate Jacobian:

$$\delta(f(P_2)) = \frac{\delta(P_2 - P_2(P_1, \theta_{12}))}{\left|\frac{\partial f}{\partial P_2}\right|}$$

$$= \frac{\delta(P_2 - P_2(P_1, \theta_{12}))}{\left|P_2\left(\frac{1}{m_2} + \frac{1}{m_3}\right) - \frac{1}{m_3}(P_o\cos\theta_2 - P_1\cos\theta_{12})\right|} \,,$$

where $P_2(P_1,\theta_{12})$ is the solution of the three-body kinematics for P_2 as a function of P_1 and θ_{12} derived previously, and θ_{12} is the angle between particles 1 and 2. Substituting this delta function in the above, integration over P_2 yields

$$N_t = \int_{P_1}\int_{\Omega_1}\int_{\Omega_2} \frac{m_3[P_2(P_1,\theta_{12})]^2 P_1^2}{\left|P_2\left(\frac{m_2+m_3}{m_2}\right) - P_o\cos\theta_2 + P_1\cos\theta_{12}\right|} dP_1 d\Omega_1 d\Omega_2$$

The integrand of this equation then serves to define the differential phase-space volume $N(P_1,\Omega_1,\Omega_2)$.

$$N(P_1,\Omega_1,\Omega_2) = \frac{m_3 P_1^2 [P_2(P_1,\theta_{12})]^2}{\left|P_2(P_1,\theta_{12})\left(\frac{m_2+m_3}{m_2}\right) - P_o\cos\theta_2 + P_1\cos\theta_{12}\right|}$$

This may be simply expressed as a function of the energy T_1:

$$N(T_1,\Omega_1,\Omega_2) = \frac{\partial P_1}{\partial T_1} N(P_1,\Omega_1,\Omega_2)$$

$$= \frac{m_1 m_3 P_1 [P_2(P_1,\theta_{12})]^2}{\left|P_2(P_1,\theta_{12})\left(\frac{m_2+m_3}{m_2}\right) - P_o\cos\theta_2 + P_1\cos\theta_{12}\right|}$$

The integrated value of N_T is given by[23]:

$$N_T = \frac{1}{2}(2\pi)^3 \left(\frac{m_1 m_2 m_3}{m_1+m_2+m_3}\right)^{3/2} \left(\frac{m_T T_o}{m_1+m_2+m_3} + Q\right)^2$$

where m_T is the mass of the target nucleus and T_o is the bombarding energy. Therefore the percentage of the total phase-space available in the energy increment ΔT_1 and solid angles $\Delta\Omega_1$ and $\Delta\Omega_2$ is given by:

$$N_1 = \frac{\int_{\Delta T_1} \int_{\Delta\Omega_1} \int_{\Delta\Omega_2} N(T_1, \Omega_1, \Omega_2)\, dT_1\, d\Omega_1\, d\Omega_2}{N_T}$$

This distribution is typically a smoothly varying curve peaked at the maximum energy kinematically allowed for particle 1.

E. The Cross-Sections for Sequential Break-Up.

In this section, the theory of sequential two-body decay of the three-body system will be given, under the assumption of incoherent decay through the various meta-stable states of the intermediate nuclei. The discussion will assume that no interference between the various mechanisms, and no interference between different manifestations of the same mechanism contribute significantly to the yield. It is convenient to introduce five different coordinate systems as follows:

1. The laboratory coordinate system, in which the experimental variables are represented by upper-case letters, the supscripts denoting the detector for the emitted particle, i.e. particle 1 in detector 1 at angles Θ_1, Φ_1. In all

cases, particle 3 is the undetected particle.

2. The three-body system center of mass, or SCM, represented by lower-case letters, with subscripts as above.

3. The different recoil center of mass (RCM) systems, corresponding to particles 1, 2, or 3 as the first emitted particle. Variables in these coordinate systems will be represented by lower-case letters, with subscripts as above, and superscripts denoting which particle is first emitted.

The reaction is assumed to proceed <u>via</u> a superposition of the following mechanisms:

$$A + B \longrightarrow C^* \longrightarrow 1 + (2,3) \longrightarrow 1 + 2 + 3 \qquad (1)$$

$$C^* \longrightarrow 2 + (1,3) \longrightarrow 1 + 2 + 3 \qquad (2)$$

$$C^* \longrightarrow 3 + (1,2) \longrightarrow 1 + 2 + 3 \qquad (3)$$

We consider the systems (2,3), (1,3), and (1,2) to be metastable states of internal energy E^1, E^2, and E^3 respectively, localized within radii r_1, r_2, and r_3. We suppose that there is unit probability that the respective metastable systems will hold together just long enough for the first emitted particle to escape the interaction radius. Under these assumptions we may write the cross-section for the first emitted particle in terms of the density of states functions (see reference 19) $\rho_1(E^1,r_1)$, $\rho_2(E^2,r_2)$, and $\rho_3(E^3,r_3)$ describing the respective recoil systems, the

Hamiltonians for each channel, and the initial and final state vectors:

$$\sigma(E^1) = \rho_1(E^1,r_1) \cdot \frac{\mu_A\mu_1 k_1}{4\pi^2 h^4 k_A} \left| \langle (2,3)+1,E^1 | H_1 | A+B,E_2 \rangle \right|^2$$

$$\sigma(E^2) = \rho_2(E^2,r_2) \cdot \frac{\mu_A\mu_2 k_2}{4\pi^2 h^4 k_A} \left| \langle (1,3)+2,E^2 | H_2 | A+B,E_A \rangle \right|^2$$

$$\sigma(E^3) = \rho_3(E^3,r_3) \cdot \frac{\mu_A\mu_3 k_3}{4\pi^2 h^4 k_A} \left| \langle (1,2)+3,E^3 | H_3 | A+B,E_A \rangle \right|^2$$

If more than one metastable state in the intermediate recoil nucleus may decay to the same final state, then the $\rho_i(E^i,r_i)$ must be considered as a sum over each channel. The channels are taken to be incoherent, so that interference between the channels is not considered. The appropriate quantum numbers for each metastable state must be inserted in order to calculate the angular dependence of the yield. We shall denote these metastable states of the intermediate nucleus by λ_i, and their appropriate quantum numbers by $\{\lambda_i\}$, where the subscript denotes the first emitted particle.

Let us consider for the moment only reaction mechanism (1). The differential cross-section of the first emitted particle in the system center of mass (SCM) may be written as:

$$\sigma_1^{\lambda_i}(E^1,\theta_1,\varphi_1) = \left| f_1^{\{\lambda_i\}}(\theta_1,\varphi_1) \right|^2 \sigma_1(E^1)$$

The angular factors $f_i^{\{\lambda_i\}}$ are treated in Appendix D. We now calculate the probability that the recoil (2,3) system with internal energy E^1 will emit particle 2 into angles $\theta_2^{(1)},\varphi_2^{(1)}$ in recoil center of mass (RCM) system 1, when particle 1 is emitted at θ_1, ϕ_1. This probability may be written as:

$$\sum_{\lambda_1} \sigma_1^{\lambda_1}(E^1) \left| f_1^{\{\lambda_1\}}(\theta_1,\varphi_1) \right|^2 \cdot \left| f_2^{\{\lambda_1\}}(\theta_2^{(1)},\varphi_2^{(1)}) \right|^2$$

where the coordinates of particle 1 are written in the SCM, while those of particle 2 are in the RCM. This expression may be transformed to the SCM by multiplication by the Jacobian $J_1 = \left| \frac{\partial(E^1,\theta_2^{(1)},\varphi_2^{(1)})}{\partial(t_1,\theta_2,\varphi_2)} \right|$, and from the SCM to the laboratory by multiplication by the Jacobian

$J_L = \left| \frac{\partial(t_1,\theta_1,\varphi_1,\theta_2,\varphi_2)}{\partial(T_1,\Theta_1,\Phi_1,\Theta_2,\Phi_2)} \right|$. These Jacobians, as well as

$J_2 = \left| \frac{\partial(E^2,\theta_2^{(2)},\varphi_2^{(2)})}{\partial(t_1,\theta_2,\varphi_2)} \right|$ and $J_3 = \left| \frac{\partial(E^3,\theta_1^{(3)},\varphi_1^{(3)}}{\partial(t_1,\theta_1,\varphi_1)} \right|$,

(appropriate for the other two sequential mechanisms) have been calculated by Bronson and Simpson (references 12 and 14), and the results are quoted below:

$$J_1 = \left| \frac{M}{m_2} \frac{(p_2)^2}{p_2^{(1)}} \left[\frac{1}{Ap_2 + p_1 \cos\delta_{12}} \right] \right|$$

$$J_2 = \left| \frac{p_1 p_2^{(1)}}{p_2 p_1^{(2)}} J_1 \right|$$

$$J_3 = \left| \frac{M}{m_2} \frac{p_1 (p_2)^2}{p_3 p_1^{(3)}} \left[\frac{1}{Ap_2 + p_1 \cos\delta_{12}} \right] \right|$$

$$J_L = \left| \frac{p_1 (p_2)^2}{p_1 (p_2)^2} \left[\frac{Ap_2 + p_1 \cos\delta_{12}}{AP_2 + P_1 \cos\textcircled{H}_{12} - P_o \cos\textcircled{H}_2} \right] \right|$$

where δ_{12} is the SCM angle between the velocity vectors for particles 1 and 2, upper-case letters represent laboratory quantities, lower-case letters without superscripts represent SCM quantities, lower-case letters with superscripts represent RCM quantities, $A = (m_2+m_3)/m_2$, and $M = m_1+m_2+m_3$.

We may now write the general expression for the cross-section under the assumptions given as:

$$\sigma = \left\{ (1+\delta_{23}) \sum_{\lambda_1} \left| f_1^{\{\lambda_1\}} (\theta_1, \varphi_1) \right|^2 \sigma_1^{\lambda_1} (E^1) \left| f_2^{\{\lambda_1\}} (\theta_2^{(1)}, \varphi_2^{(1)}) \right|^2 J_1 J_L \right\}$$

$$+ \left\{ (1+\delta_{13}) \sum_{\lambda_2} \left| f_1^{\{\lambda_2\}} (\theta_1, \varphi_1) \right|^2 \sigma_2^{\lambda_2} (E^2) \left| f_2^{\{\lambda_2\}} (\theta_2^{(2)}, \varphi_2^{(2)}) \right|^2 J_2 J_L \right\}$$

$$+ \left\{ (1+\delta_{12}) \sum_{\lambda_3} \left| f_1^{\{\lambda_3\}} (\theta_3, \varphi_3) \right|^2 \sigma_3^{\lambda_3} (E^3) \left| f_2^{\{\lambda_3\}} (\theta_1^{(3)}, \varphi_1^{(3)}) \right|^2 J_3 J_L \right\}$$

where $\delta_{ij} = 1$ if particles i and j are identical, and zero otherwise. This expression must be integrated over the experimental solid angles and size of the target spot in order to predict the observed yield.

Details of the calculation of the density of states functions are given in the next section, and in Appendix C. The angular dependence is treated in Appendix D.

F. Density of States Functions

The generalized density of states functions have been treated in detail by Phillips and his co-workers[19]. For a system which has only sharp bound states of energies E_n, the density of states function is given by:

$$\rho(E^1) = \sum_n \delta(E^1 - E_n)$$

The extension to continuum states is made by arguing that the probability for particle 1 to be emitted to produce a continuum state (2,3) is proportional to the probability that 1 and 2 be localized within a spherical volume of radius r_1, which includes the interaction volume of 1 with (2,3). This probability is calculated from the wave function of the relative motion:

$$\Psi = N(E^1)\ [U(E^1,r)/r]\ Y_{\ell}^{m}\ (\theta_2^{(1)},\varphi_2^{(1)})$$

where $U(E^1,r)/r$ is the radial wave function normalized in the spherical volume of radius r_1. The factor $N(E^1)$ relates the generalized density of states function to the usual density of states function $\rho_o = \mu r_1/\pi h^2 k_1$ through the relation:

$$\rho(E^1,r_1) = \rho_o(E^1)N^2(E^1)$$

Applying the normalized external wave function for the ℓ^{th} partial wave $U_\ell = (2/r_1)^{1/2} A_\ell \sin(\delta_\ell + \varphi_\ell)$, the renormalized density of states function is given by:

$$\rho_\ell(E^1,r_1) = \frac{\mu_2}{\pi h^2 k_2}\left[\frac{d}{dk_2}(\delta_\ell+\varphi_\ell) - \frac{1}{2}\left(\frac{1}{k_2} - \frac{2\frac{\partial A_\ell}{\partial k_2}}{A_\ell}\right)\sin 2(\delta_\ell+\varphi_\ell)\right.$$

$$\left. - \frac{1}{k_2}\left(A_\ell \frac{\partial^2 A_\ell}{\partial k_2 \partial r} - \frac{\partial A_\ell}{\partial r}\frac{\partial A_\ell}{\partial k_2}\sin^2(\delta_\ell+\varphi_\ell)\right)\right]$$

where δ_ℓ and φ_ℓ are the ℓ^{th} wave nuclear and hard sphere phase shifts respectively for the scattering of particle 2 from 3, and $A_\ell = (F_\ell^2 + G_\ell^2)^{1/2}$, with $F_\ell(E^1,r_1)$ and $G_\ell(E^1,r_1)$ the regular and irregular partial wave solutions for the coulomb scattering of 2 from 3. The hard sphere phase shift is given by:

$$\varphi_\ell(E^1,r_1) = \tan^{-1}(F_\ell/G_\ell)$$

For the case in which U_ℓ is independent of energy in the region $r \lesssim r_1$, the above expression reduces to:

$$\rho_\ell(E^1, r_1) = \text{constant } (\sin^2(\delta_\ell + \varphi_\ell)/P_\ell)$$

where $P_\ell = k_2 r_1 / A_\ell^2$ is the penetrability factor for the ℓ^{th} partial wave. This result has also been obtained by Watson[17] by a time reversal argument.

The details of the calculation of these functions for metastable states in ^{8}Be and ^{6}Li are given in Appendix C.

IV. EXPERIMENTAL DATA

Figures 10, 11, and 12 present typical energy-energy spectra in the form of rough contour maps with different plotting symbols indicating different yield intensities. The Et^2 method has been used to identify the particle in detector 1 as either a deuteron or an alpha particle, and histograms of the yield projected on the energy axis of the identified particle are shown below the contour maps. The yield in each cell of the contour maps represents the differential cross-section $d^4\sigma/d\Omega_1 d\Omega_2 dT_1 dT_2$ multiplied by the cell "volume" $\Delta T_1 \Delta T_2 \Delta\Omega_1 \Delta\Omega_2$, where ΔT_1 and ΔT_2 represent the energy widths of the cells, and $\Delta\Omega_1$ and $\Delta\Omega_2$ are the experimental solid angles. For convenience, the gain settings of the amplifiers were adjusted to 1 MeV/100 channels in the 1,000 channel configuration. The sorting program then grouped the data 10 channels per cell. Thus the final energy-energy spectra are presented in 100 x 100 cell form, with each cell 0.1 MeV in width.

The histograms of the projected yield as a function of the identified-particle energy represent a differential cross-section $d^3\sigma/dT_1 d\Omega_1 d\Omega_2$ times the "volume" $\Delta T_1 \Delta\Omega_1 \Delta\Omega_2$. The absolute cross-section measurements were made using the technique described in section II-E. The strong

Figure 10. Contour maps of energy-energy spectra for particle 1 identified alternately as a deuteron, or as an alpha particle. The histograms are integrated projections of the intensity on the energy axis of the identified particle. Strong final state interactions through the 2.184 MeV state in ^{6}Li and the 2.90 MeV state in ^{8}Be are evident. The cross-hatched region indicates that portion of the α-d and α-α loci which could not be resolved without ambiguity.

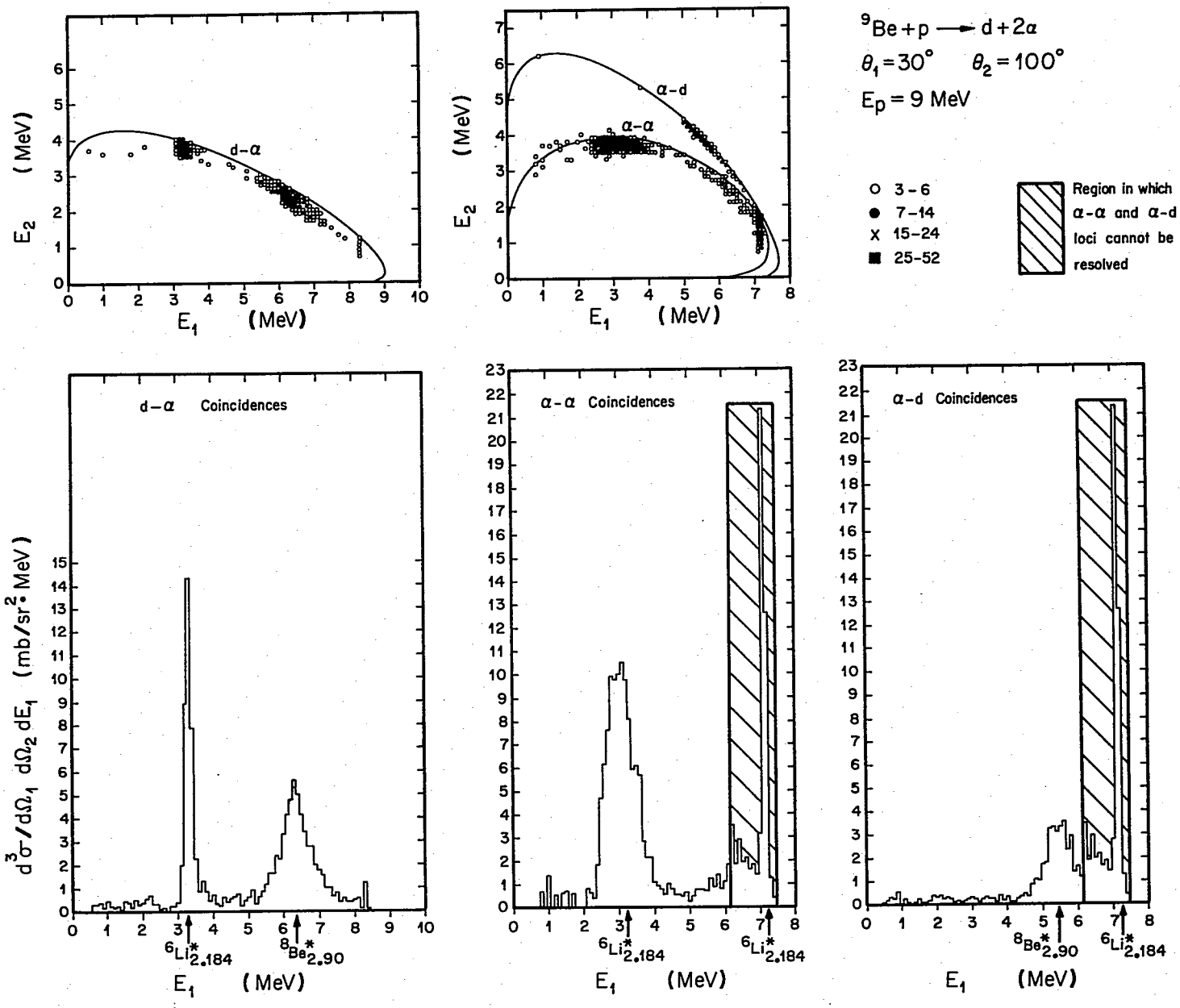
$^9Be + p \longrightarrow d + 2\alpha$
$\theta_1 = 30°$ $\theta_2 = 100°$
$E_p = 9$ MeV
d–α
α–α
α–d
E_2 (MeV)
E_1 (MeV)
3 - 6
7 - 14
15 - 24
25 - 52
Region in which α–α and α–d loci cannot be resolved
d–α Coincidences
α–α Coincidences
α–d Coincidences
$d^3\sigma/d\Omega_1\, d\Omega_2\, dE_1$ (mb/sr^2·MeV)
$^6Li^*_{2.184}$
$^8Be^*_{2.90}$

Figures 11 and 12. Contour maps similar to figure 10. In addition to the final state interactions previously mentioned, a strong yield through the ^{8}Be ground state is evident.

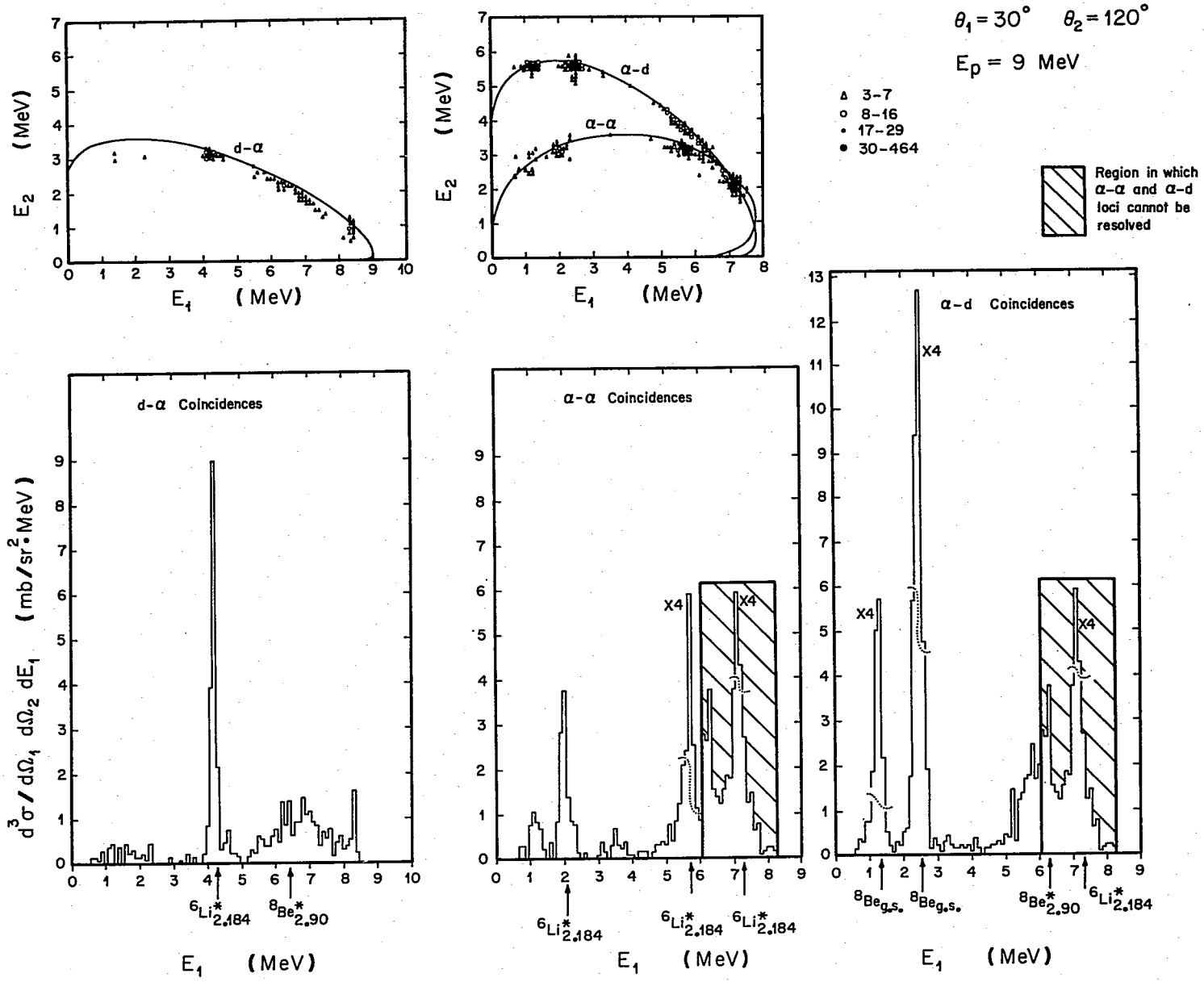
$^9Be + p \rightarrow d + 2\alpha$
$\theta_1 = 30°$ $\theta_2 = 120°$
$E_p = 9$ MeV
Δ 3-7
○ 8-16
• 17-29
● 30-464
Region in which α-α and α-d loci cannot be resolved
d-α
α-d
α-α
E_2 (MeV)
E_1 (MeV)
d-α Coincidences
α-α Coincidences
α-d Coincidences
$d^3\sigma / d\Omega_1\, d\Omega_2\, dE_1$ (mb/sr^2·MeV)
X4
$^6Li^*_{2.184}$
$^8Be^*_{2.90}$
$^8Be_{g.s.}$

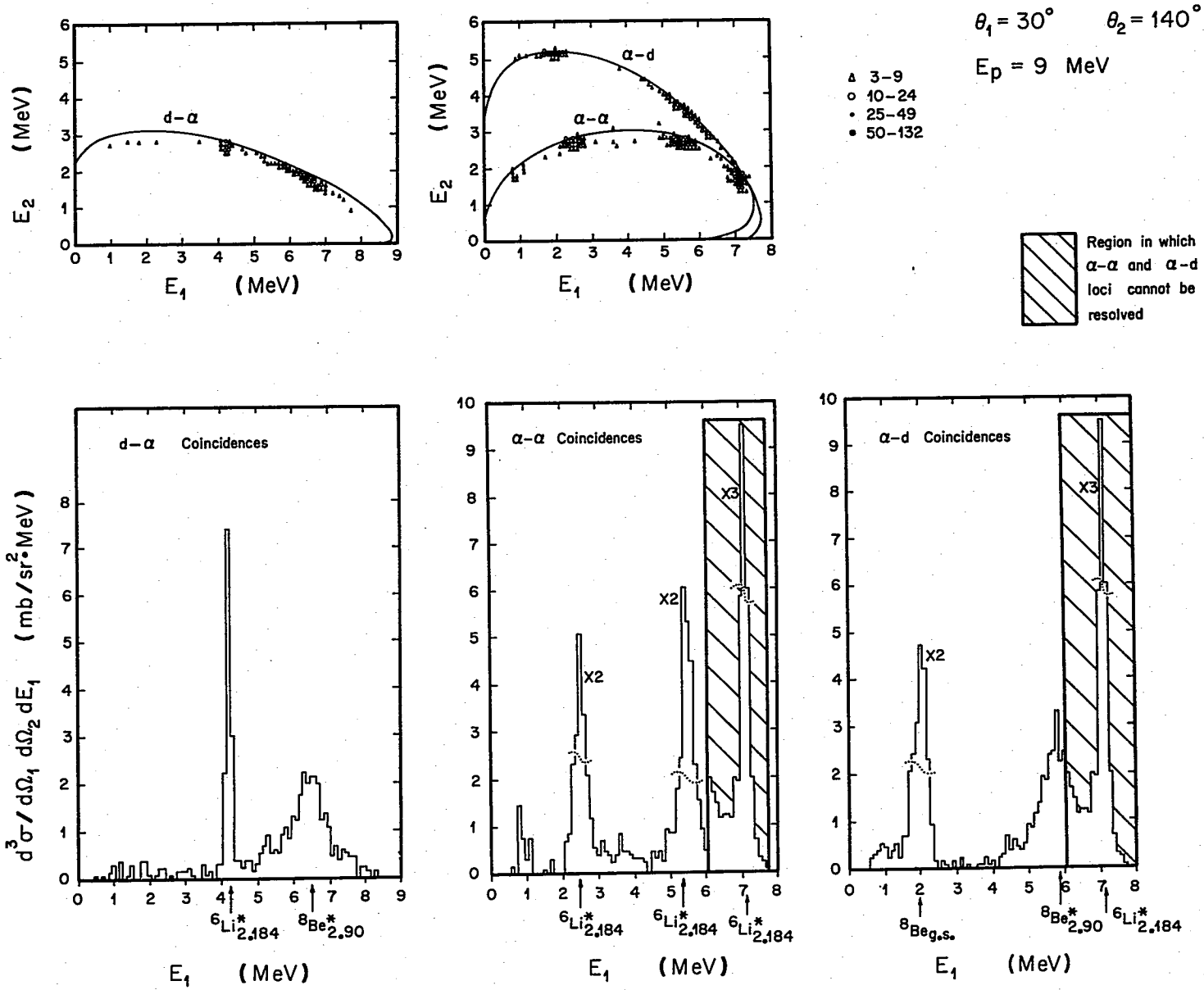
$^9Be + p \rightarrow d + 2\alpha$
$\theta_1 = 30°$ $\theta_2 = 140°$
$E_p = 9$ MeV
△ 3-9
○ 10-24
• 25-49
● 50-132
d-α
α-d
α-α
E_2 (MeV)
E_1 (MeV)
Region in which α-α and α-d loci cannot be resolved
d-α Coincidences
α-α Coincidences
α-d Coincidences
$d^3\sigma / d\Omega_1\, d\Omega_2\, dE_1$ (mb/sr^2·MeV)
X2
X3
$^6Li^*_{2.184}$
$^8Be^*_{2.90}$
$^8Be_{g.s.}$

peaks due to final state interactions in metastable states of ^{8}Be and ^{6}Li are identified on each histogram.

Figures 10, 11 and 12 show strong evidence of sequential decay *via* the 2.184 MeV state in ^{6}Li and the 2.90 MeV state in ^{8}Be. In addition, the spectra of alpha-d coincidences of figures 11 and 12 show large peaks due to final state interactions in the ground state of ^{8}Be.

A better overall view of the extent to which these final state interactions dominate the yield can be had from figures 13-24. These figures present in isometric view, families of histograms of yield projected on the identified-particle axis, as a function of the angle of the detector of the unidentified particle. The smooth curves indicate the positions where peaking due to sequential decay through the indicated metastable states is expected. In addition to the states mentioned above, the expected positions of the 4.57 MeV state in ^{6}Li are also shown, although the evidence for sequential decay *via* this channel is weak. The cross-hatched regions on both the histograms and the isometric figures indicate regions in which the alpha-d and alpha-alpha kinematic loci were not sufficiently separated that a positive determination of the yield on each locus could be made. This difficulty could be overcome by doing particle-identification on both coincident particles, but the present

Figures 13, 14, 15, 16. Isometric drawings of families of d-alpha histograms, for deuteron angles of 20°, 30°, 40°, and 50°. The smooth curves indicate the expected positions of enhanced yield due to final state interactions in the indicated states.

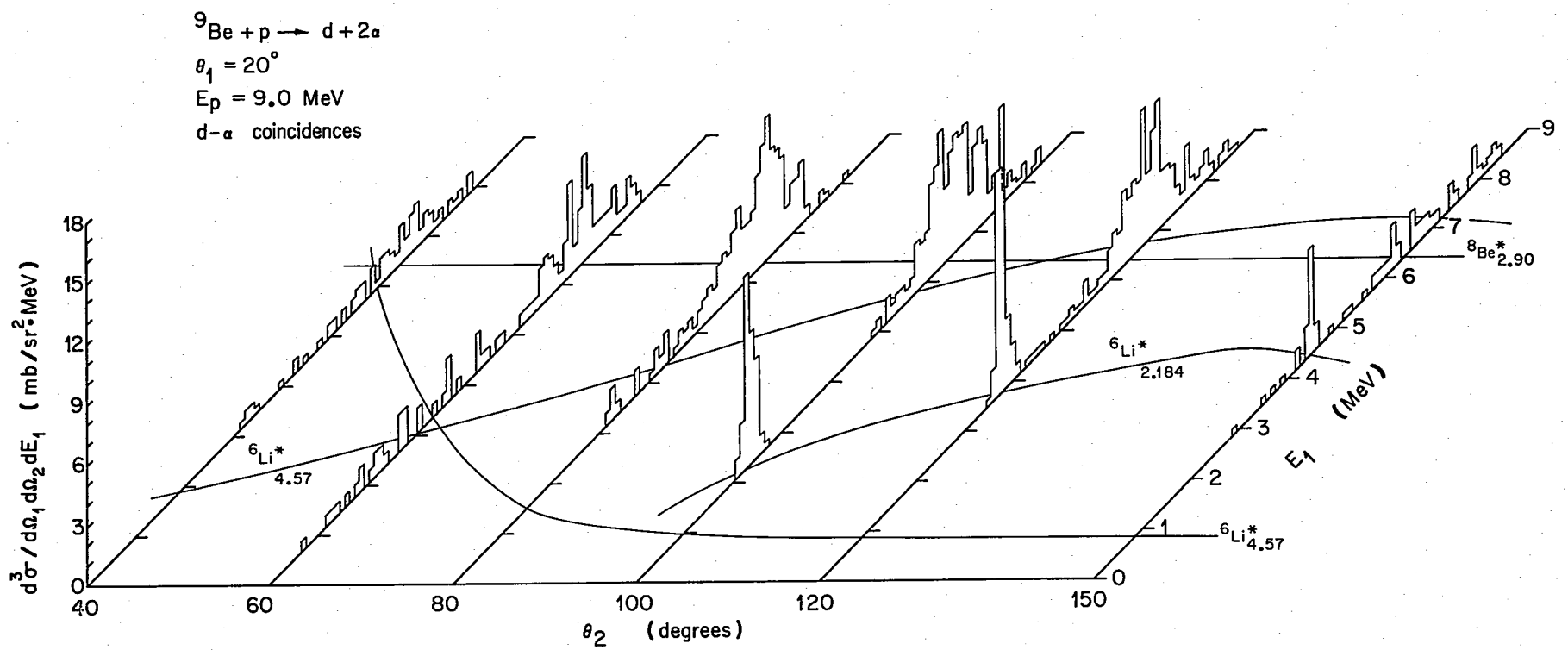
^{9}Be + p → d + 2α
θ_1 = 20°
E_p = 9.0 MeV
d-α coincidences
$d^3\sigma / d\Omega_1 d\Omega_2 dE_1$ (mb/sr^2•MeV)
θ_2 (degrees)
E_1 (MeV)
^{6}Li*
4.57
^{6}Li*
2.184
^{8}Be*$_{2.90}$
^{6}Li*$_{4.57}$

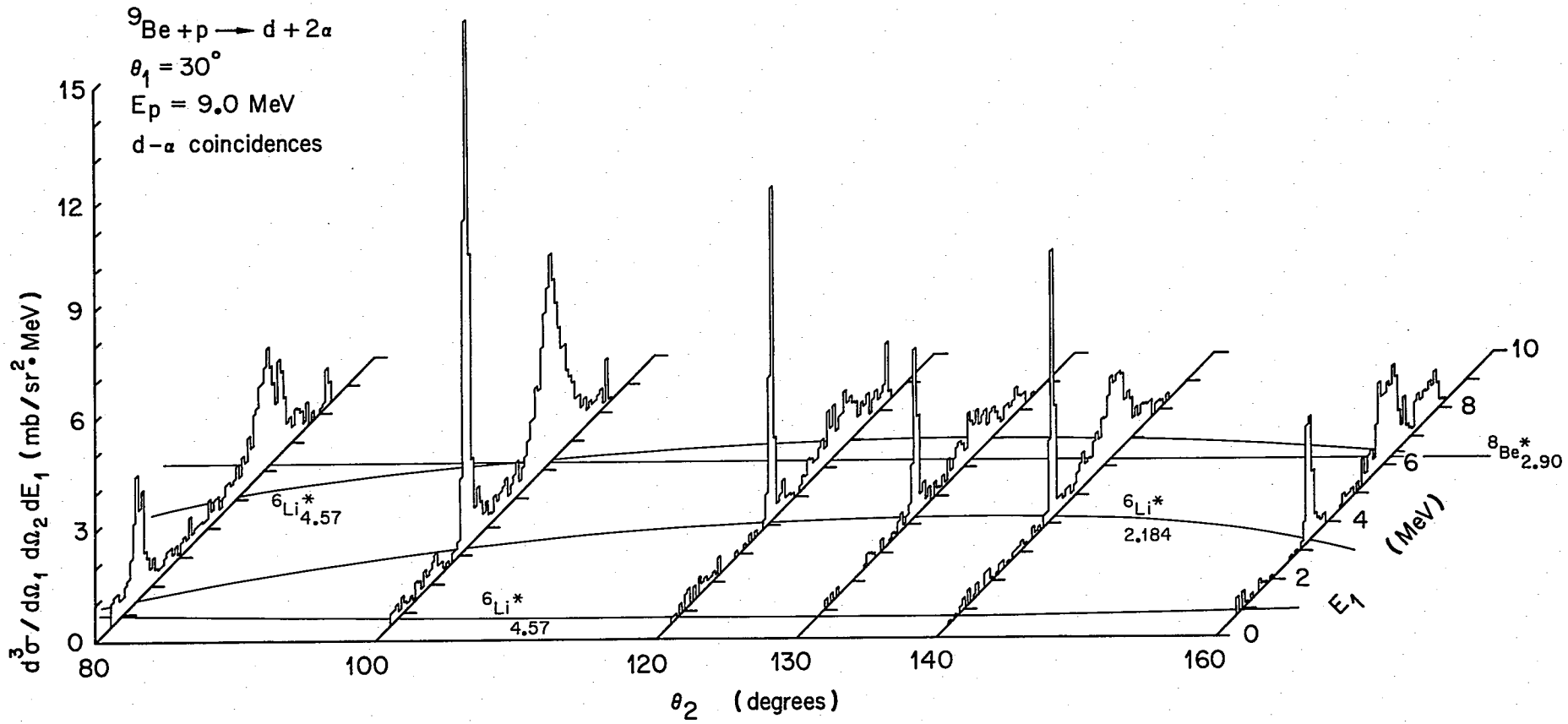
^{9}Be + p ⟶ d + 2α
θ_1 = 30°
E_p = 9.0 MeV
d − α coincidences
$d^3\sigma / d\Omega_1\, d\Omega_2\, dE_1$ (mb/sr^2·MeV)
15
12
9
6
3
0
80
100
120
130
140
160
θ_2 (degrees)
^{6}Li*$_{4.57}$
^{6}Li*
4.57
^{6}Li*
2.184
^{8}Be*$_{2.90}$
10
8
6
4
2
0
E_1 (MeV)

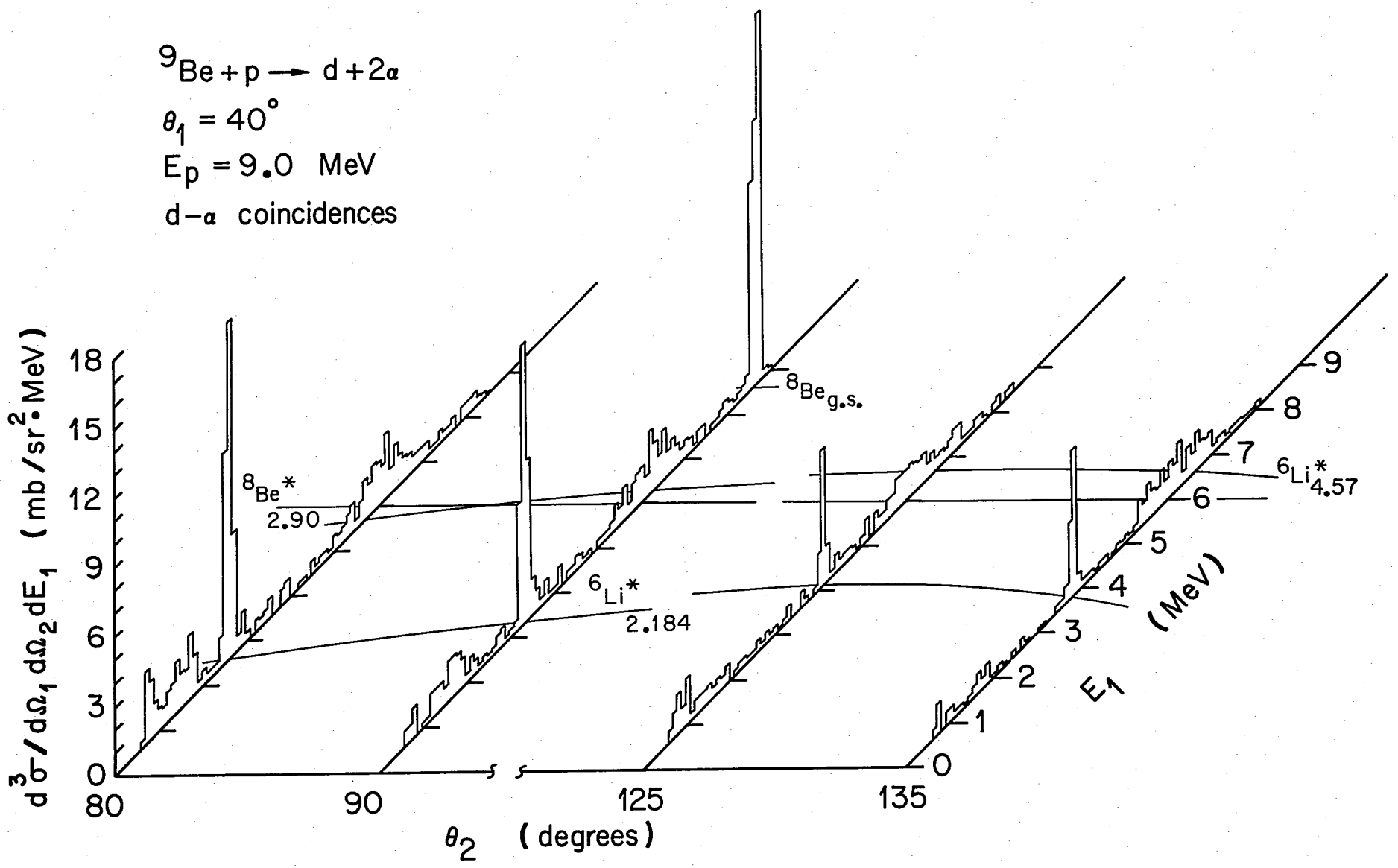
$^9Be + p \rightarrow d + 2\alpha$
$\theta_1 = 40^\circ$
$E_p = 9.0$ MeV
d–α coincidences
$d^3\sigma / d\Omega_1 d\Omega_2 dE_1$ (mb/sr^2•MeV)
0
3
6
9
12
15
18
$^8Be^*$
2.90
$^8Be_{g.s.}$
$^6Li^*$
2.184
$^6Li^*_{4.57}$
0
1
2
3
4
5
6
7
8
9
E_1 (MeV)
80
90
125
135
θ_2 (degrees)

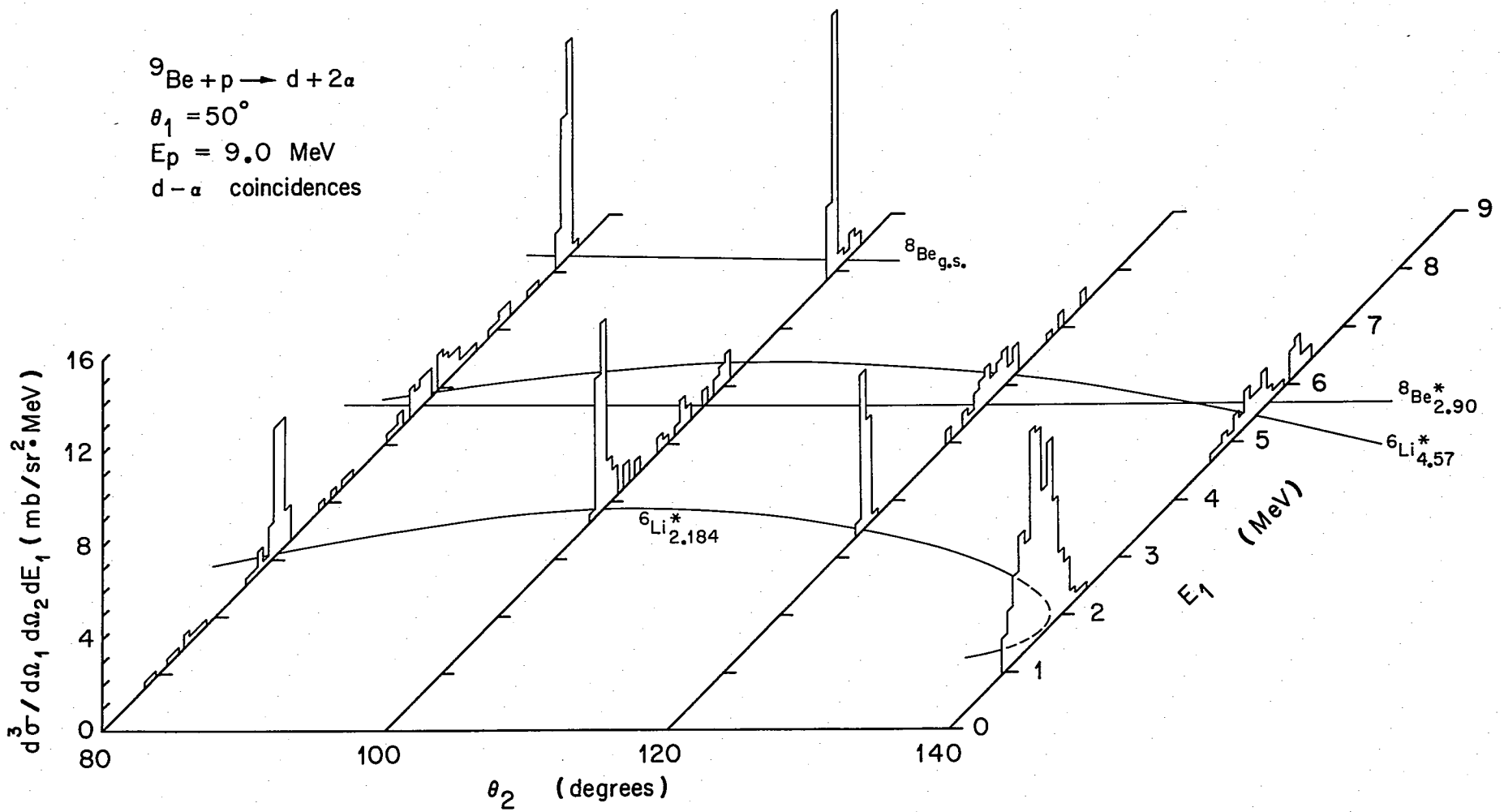
$^{9}Be + p \rightarrow d + 2\alpha$
$\theta_1 = 50°$
$E_p = 9.0$ MeV
$d - \alpha$ coincidences
$^{8}Be_{g.s.}$
$^{8}Be^{*}_{2.90}$
$^{6}Li^{*}_{4.57}$
$^{6}Li^{*}_{2.184}$
$d^3\sigma / d\Omega_1 \, d\Omega_2 \, dE_1$ (mb / sr^2 • MeV)
θ_2 (degrees)
E_1 (MeV)
0
4
8
12
16
80
100
120
140
1
2
3
5
6
7
8
9

Figures 17, 18, 19, 20. Isometric drawings for families of alpha-d histograms, for alpha angles of 20°, 30°, 40°, and 50°. The cross-hatched region indicates that portion of the alpha-d locus which was not unambiguously resolved from the alpha-alpha locus.

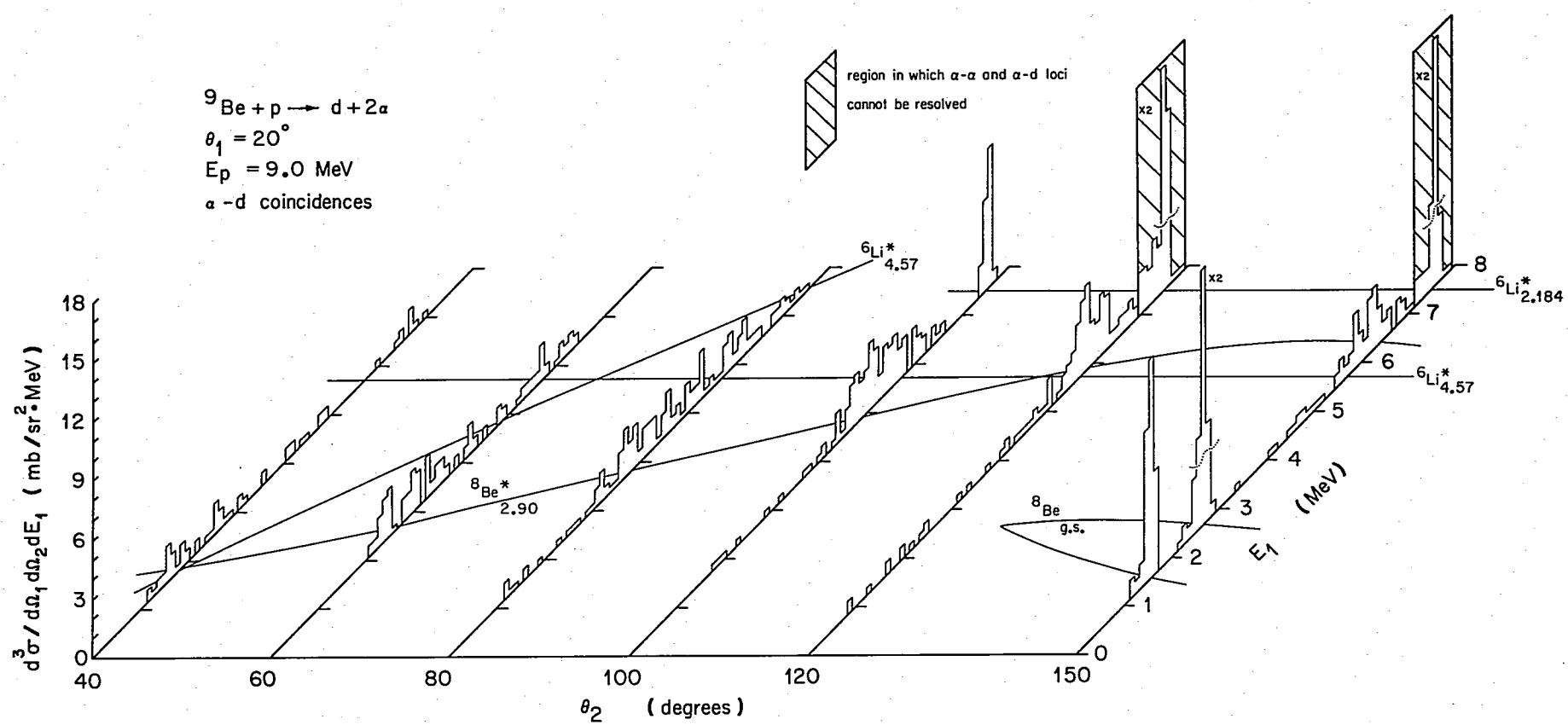
^{9}Be + p ⟶ d + 2α
θ_1 = 20°
E_p = 9.0 MeV
α -d coincidences
region in which α-α and α-d loci cannot be resolved
x2
x2
x2
^{6}Li* 4.57
^{8}Be* 2.90
^{8}Be g.s.
^{6}Li* 2.184
^{6}Li* 4.57
$d^3\sigma / d\Omega_1 d\Omega_2 dE_1$ (mb/sr^2·MeV)
0
3
6
9
12
15
18
40
60
80
100
120
150
θ_2 (degrees)
0
1
2
3
4
5
6
7
8
E_1 (MeV)

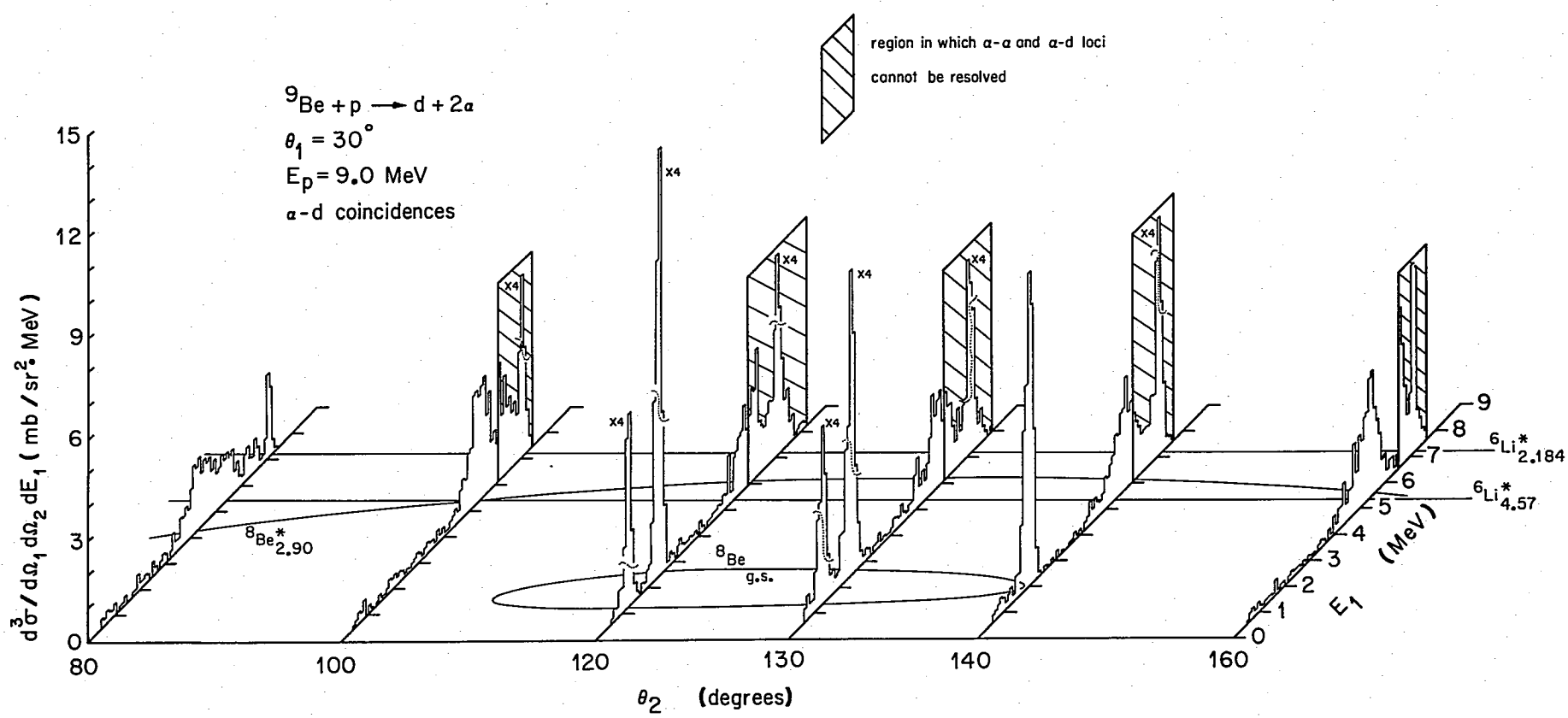
region in which α-α and α-d loci
cannot be resolved
$^9Be + p \longrightarrow d + 2\alpha$
$\theta_1 = 30^\circ$
$E_p = 9.0$ MeV
α-d coincidences
$d^3\sigma / d\Omega_1 d\Omega_2 dE_1$ (mb / sr^2 MeV)
θ_2 (degrees)
E_1 (MeV)
$^8Be^*_{2.90}$
$^8Be_{g.s.}$
$^6Li^*_{2.184}$
$^6Li^*_{4.57}$
x4

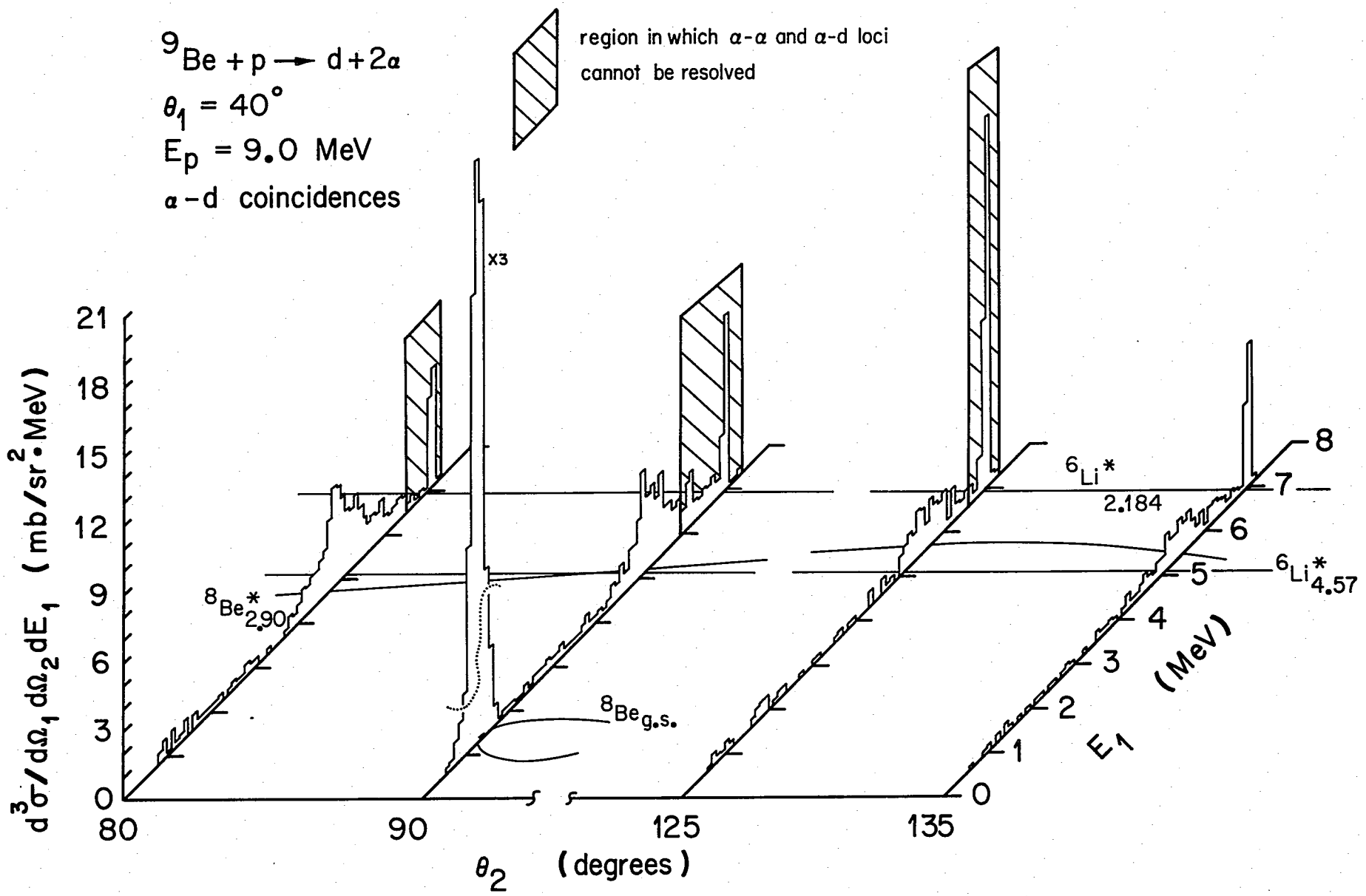
^{9}Be + p → d + 2α
θ_1 = 40°
E_p = 9.0 MeV
α-d coincidences
region in which α-α and α-d loci cannot be resolved
x3
^{8}Be*$_{2.90}$
^{8}Be$_{g.s.}$
^{6}Li*
2.184
^{6}Li*$_{4.57}$
$d^3\sigma/d\Omega_1 d\Omega_2 dE_1$ (mb/sr^2·MeV)
0
3
6
9
12
15
18
21
80
90
125
135
θ_2 (degrees)
0
1
2
3
4
5
6
7
8
E_1 (MeV)

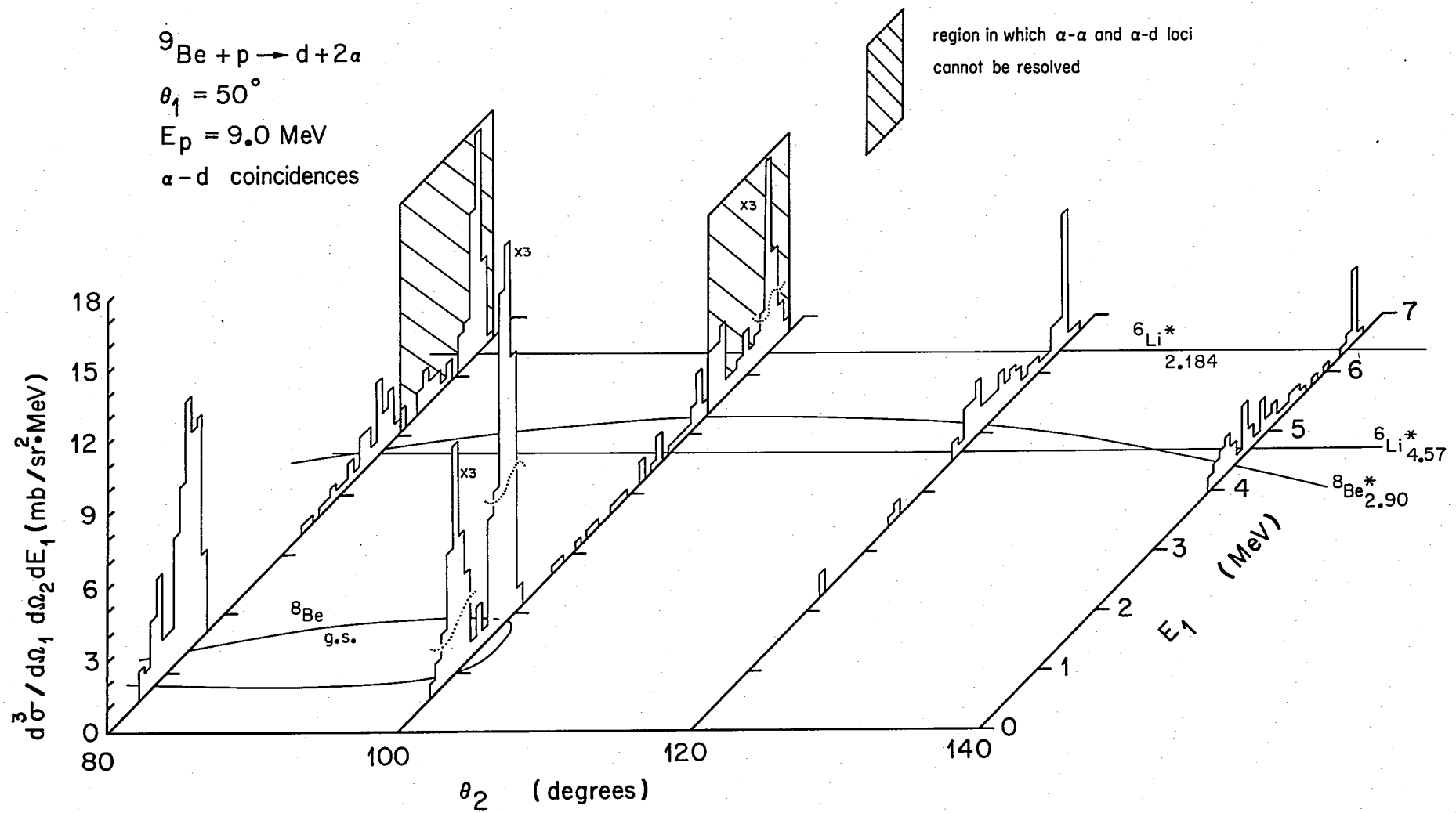
^{9}Be + p → d + 2α
θ_1 = 50°
E_p = 9.0 MeV
α - d coincidences
region in which α-α and α-d loci cannot be resolved
X3
X3
X3
^{6}Li* 2.184
^{6}Li* 4.57
^{8}Be* 2.90
^{8}Be g.s.
$d^3\sigma / d\Omega_1\, d\Omega_2 dE_1$ (mb/sr^2•MeV)
0
3
6
9
12
15
18
80
100
120
140
θ_2 (degrees)
0
1
2
3
4
5
6
7
E_1 (MeV)

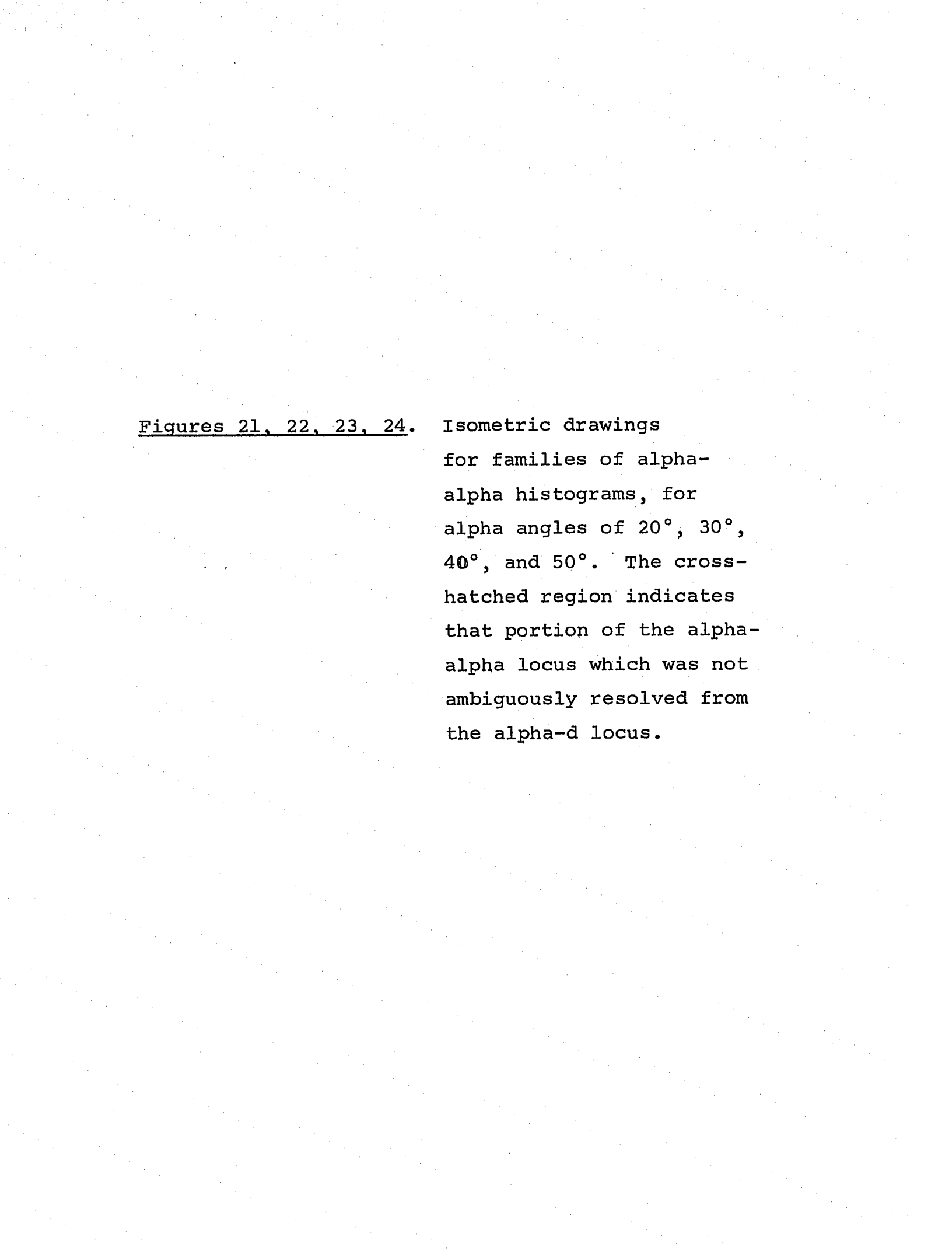

Figures 21, 22, 23, 24. Isometric drawings for families of alpha-alpha histograms, for alpha angles of 20°, 30°, 40°, and 50°. The cross-hatched region indicates that portion of the alpha-alpha locus which was not ambiguously resolved from the alpha-d locus.

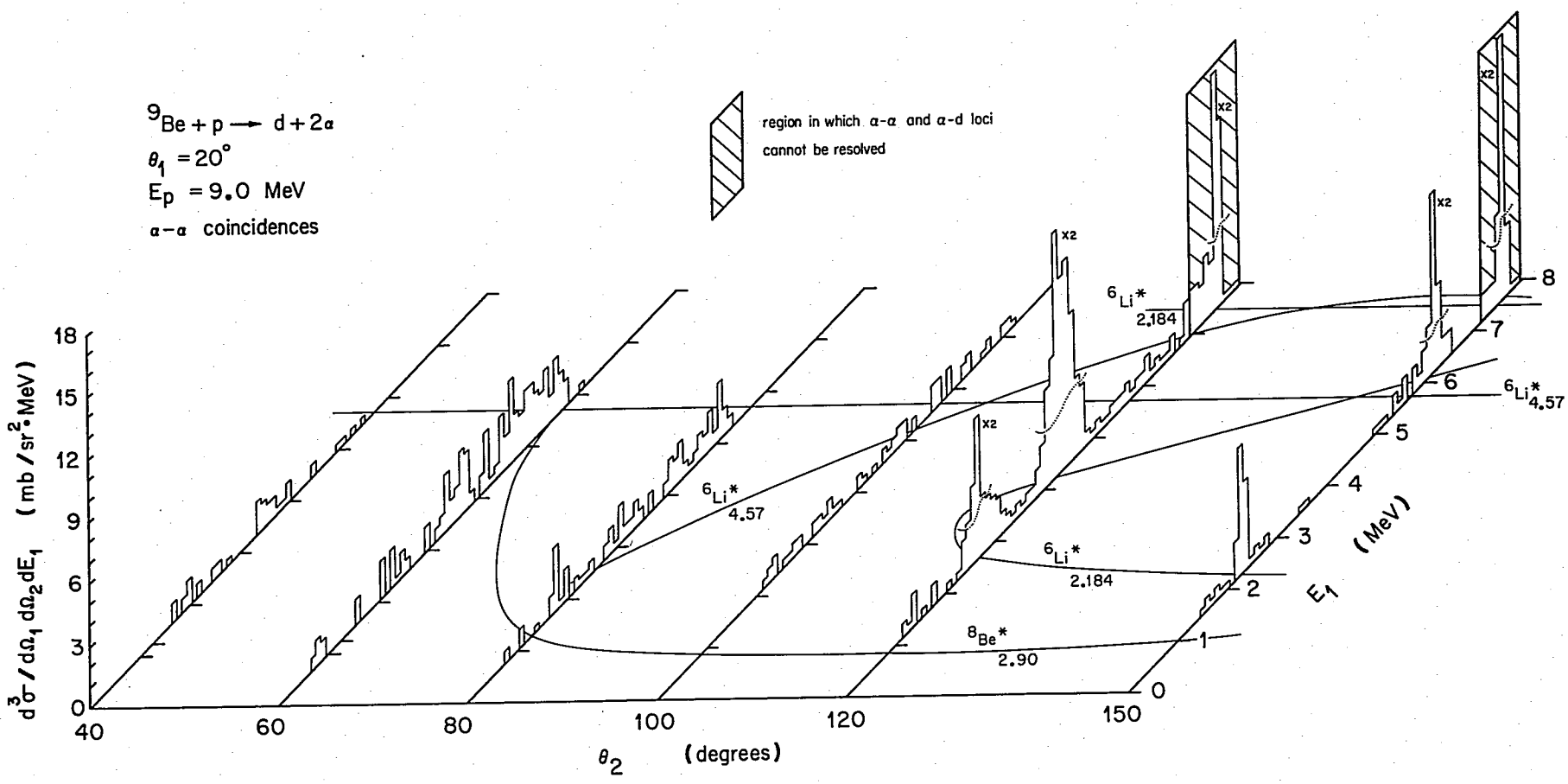
$^9Be + p \rightarrow d + 2\alpha$
$\theta_1 = 20°$
$E_p = 9.0$ MeV
$\alpha-\alpha$ coincidences
region in which α-α and α-d loci cannot be resolved
$d^3\sigma / d\Omega_1\, d\Omega_2 dE_1$ (mb / sr^2•MeV)
θ_2 (degrees)
E_1 (MeV)
$^6Li^*$ 2.184
$^6Li^*$ 4.57
$^8Be^*$ 2.90
x2

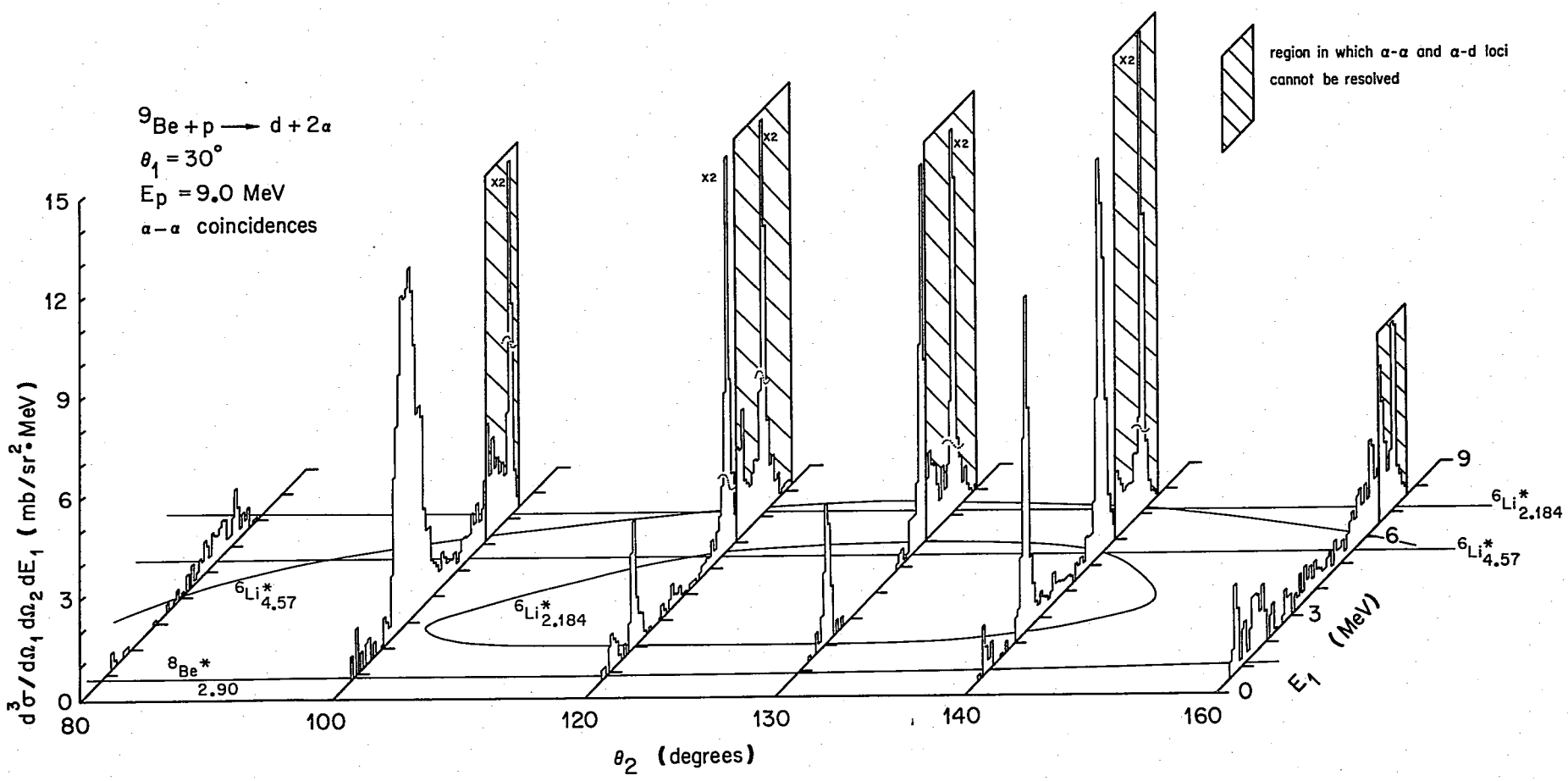
$^9Be + p \longrightarrow d + 2\alpha$
$\theta_1 = 30°$
$E_p = 9.0$ MeV
$\alpha - \alpha$ coincidences
region in which α-α and α-d loci cannot be resolved
x2
$^6Li^*_{4.57}$
$^6Li^*_{2.184}$
$^8Be^*$ 2.90
$d^3\sigma/d\Omega_1 d\Omega_2 dE_1$ (mb/sr^2•MeV)
θ_2 (degrees)
E_1 (MeV)
0
3
6
9
12
15
80
100
120
130
140
160

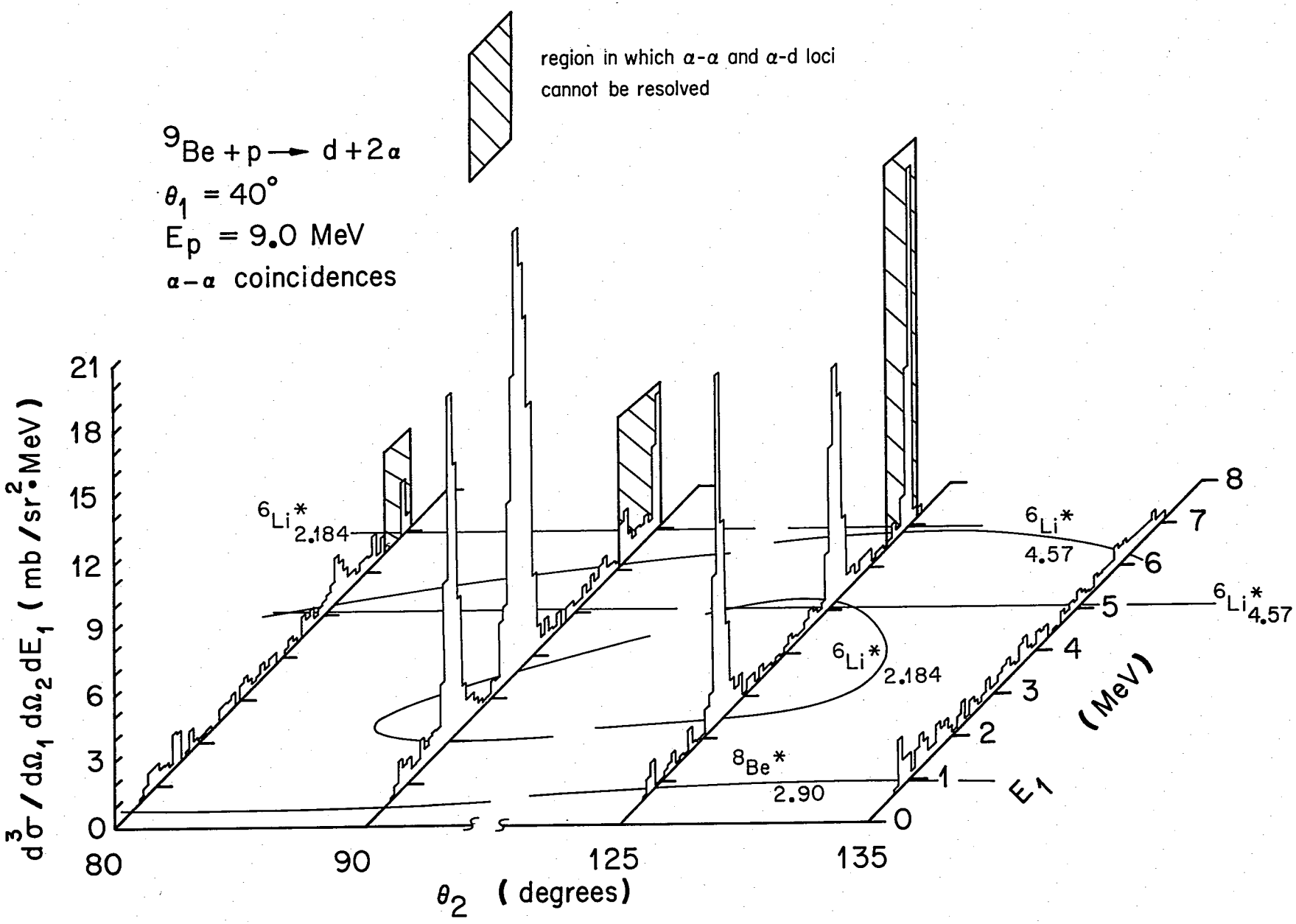
region in which α-α and α-d loci cannot be resolved
$^{9}Be + p \rightarrow d + 2\alpha$
$\theta_1 = 40°$
$E_p = 9.0$ MeV
α−α coincidences
$^{6}Li^{*}_{2.184}$
$^{6}Li^{*}_{4.57}$
$^{8}Be^{*}_{2.90}$
$d^3\sigma / d\Omega_1 d\Omega_2 dE_1$ (mb / sr^2 • MeV)
21
18
15
12
9
6
3
0
80
90
125
135
θ_2 (degrees)
E1 (MeV)
8
7
6
5
4
3
2
1
0

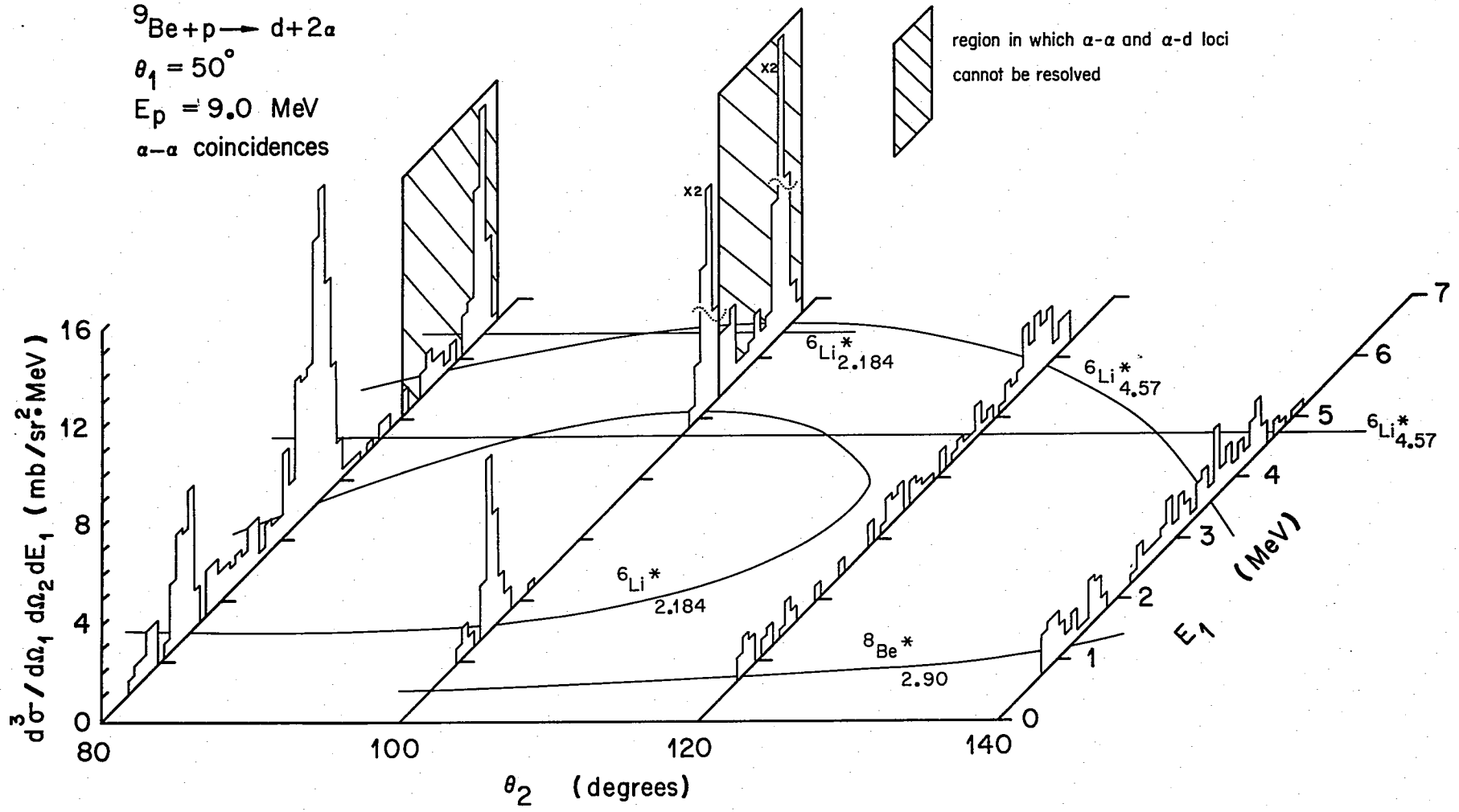
$^9Be + p \rightarrow d + 2\alpha$
$\theta_1 = 50°$
$E_p = 9.0$ MeV
$\alpha-\alpha$ coincidences
region in which $\alpha-\alpha$ and α-d loci cannot be resolved
x2
x2
$^6Li^*_{2.184}$
$^6Li^*_{4.57}$
$^6Li^*_{4.57}$
$^6Li^*$ 2.184
$^8Be^*$ 2.90
$d^3\sigma / d\Omega_1 d\Omega_2 dE_1$ (mb/sr^2·MeV)
16
12
8
4
0
80
100
120
140
θ_2 (degrees)
0
1
2
3
4
5
6
7
E_1 (MeV)

data are sufficient to determine a great deal about the reaction mechanisms.

The striking impression of all these data is that wherever decay <u>via</u> the 2.184 MeV state in ^{6}Li or the ground state or 2.90 MeV state of ^{8}Be is kinematically allowed, a large enhancement of yield is observed. In other regions there is little or no yield. The reaction is dominated by sequential decay through metastable states in the intermediate nuclei, and no evidence is seen for a significant yield due to simultaneous three-body disintegration.

V. RESULTS AND CONCLUSIONS

As has already been indicated, the experimental data are dominated by strong final state interactions through the ground state and first excited state of ^{8}Be, and through the 2.184 MeV first excited state of ^{6}Li. No conclusive evidence of decay through the ^{6}Li state at 4.57 MeV is present.

Figures 25 and 26 present density of states fits to sample spectra in which the final state interactions through all of these channels are seen. The $\sin^2(\delta_\ell+\phi_\ell)/P_\ell$ form of the density of states was used in these calculations. The renormalized form of the density of states did not reproduce the shape of the spectra as well as did the $\sin^2(\delta_\ell+\phi_\ell)/P_\ell$ form. The remarkable fits to the shape of these spectra indicate that the density of states factors are able to reproduce accurately the final state interaction amplitude as a function of excitation energy.

Figures 27 and 28 represent attempts to fit the angular dependence of the ^{6}Li 2.184 MeV state and the ^{8}Be 2.90 MeV state, for a fixed deuteron detection angle of 30°. The angular factors are given with each figure. The angle β is the angle between the recoil axis and the detected particle from the ^{6}Li or ^{8}Be break-up respectively, as seen

Figure 25. Density of states fit to the d-alpha yield for $\theta_d = 30°$, $\theta_\alpha = 100°$. The two large peaks are due to final state interactions in the ^{6}Li 2.184 MeV state and the ^{8}Be 2.90 MeV state. The small peak on the high energy end of the spectrum is due to the rapidly rising phase-space in this region of the locus, and the observed yield at this point is a sensitive function of the energy threshold of the alpha particle detector.

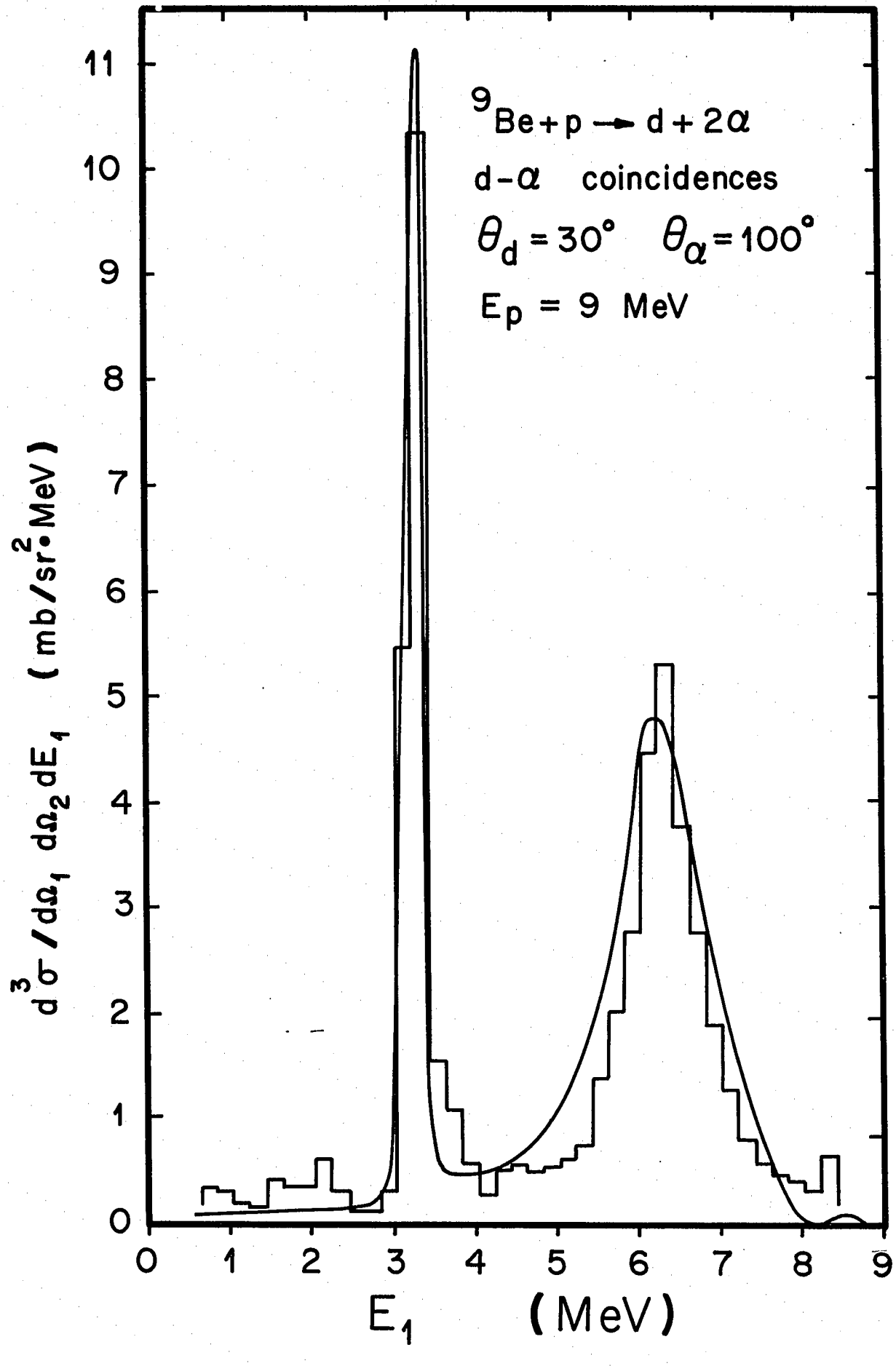
^{9}Be+p → d+2α
d-α coincidences
$\theta_d = 30°$ $\theta_\alpha = 100°$
E_p = 9 MeV
$d^3\sigma / d\Omega_1\, d\Omega_2\, dE_1$ (mb/sr^2•MeV)
E_1 (MeV)
0
1
2
3
4
5
6
7
8
9
10
11

Figure 26. Density of states fit to the alpha-d yield for $\theta = 120°$, $\theta_d = 30°$. The two sharp peaks near the low energy end of the spectrum are due to the ^{8}Be ground state, the broad peak is due to the ^{8}Be 2.90 MeV state, and the sharp peak near the high energy end of the spectrum is due to the ^{6}Li 2.184 MeV state.

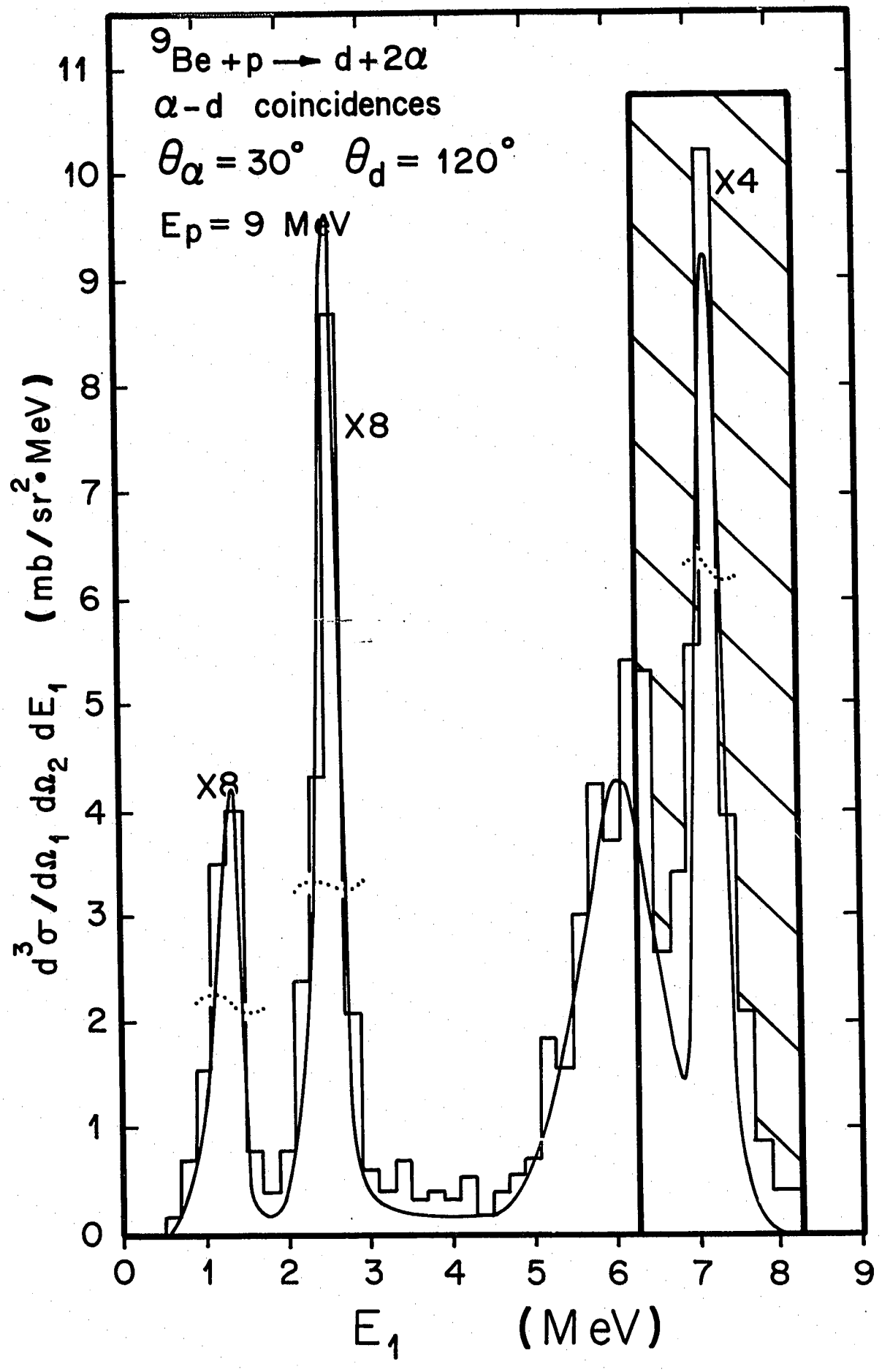
^{9}Be + p → d + 2α
α - d coincidences
$\theta_\alpha = 30°$ $\theta_d = 120°$
$E_p = 9$ MeV
X4
X8
X8
$d^3\sigma / d\Omega_1\, d\Omega_2\, dE_1$ (mb / sr^2 • MeV)
E_1 (MeV)
0
1
2
3
4
5
6
7
8
9
10
11

Figure 27. Plot of the integrated yield of the ^{6}Li 2.184 MeV state, together with the least square fit to the angular dependence. β is the angle between the detected deuteron and the ^{6}Li recoil axis in the ^{6}Li recoil center of mass system.

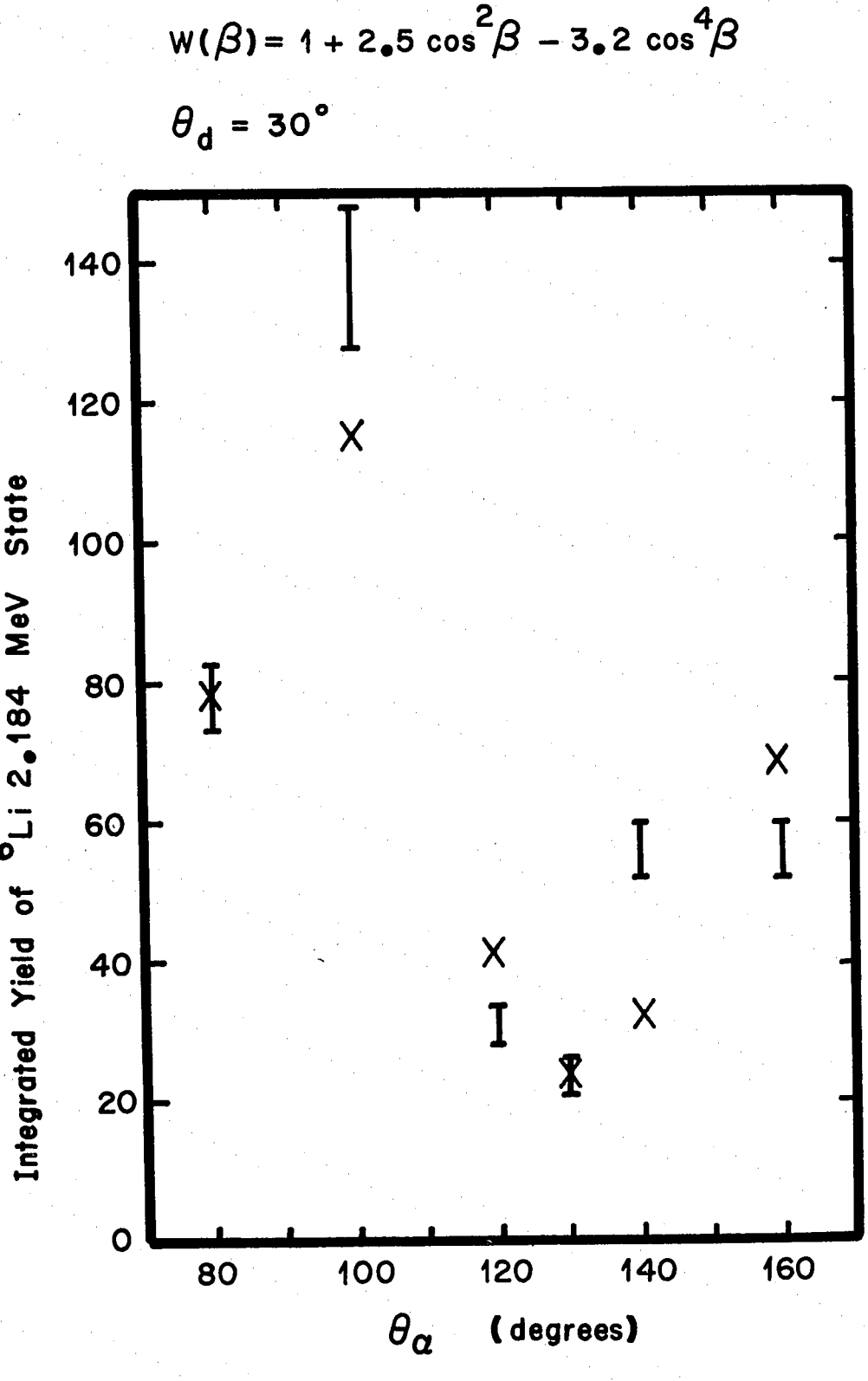
$W(\beta) = 1 + 2.5\cos^2\beta - 3.2\cos^4\beta$
$\theta_d = 30°$
Integrated Yield of ^{6}Li 2.184 MeV State
0
20
40
60
80
100
120
140
80
100
120
140
160
θ_α (degrees)

Figure 28. Plot of experimental intensity of the ^{8}Be 2.90 MeV state, together with the least square fit to the angular dependence. β is the angle between the detected alpha particle and the ^{8}Be recoil axis in the recoil ^{8}Be center of mass system.

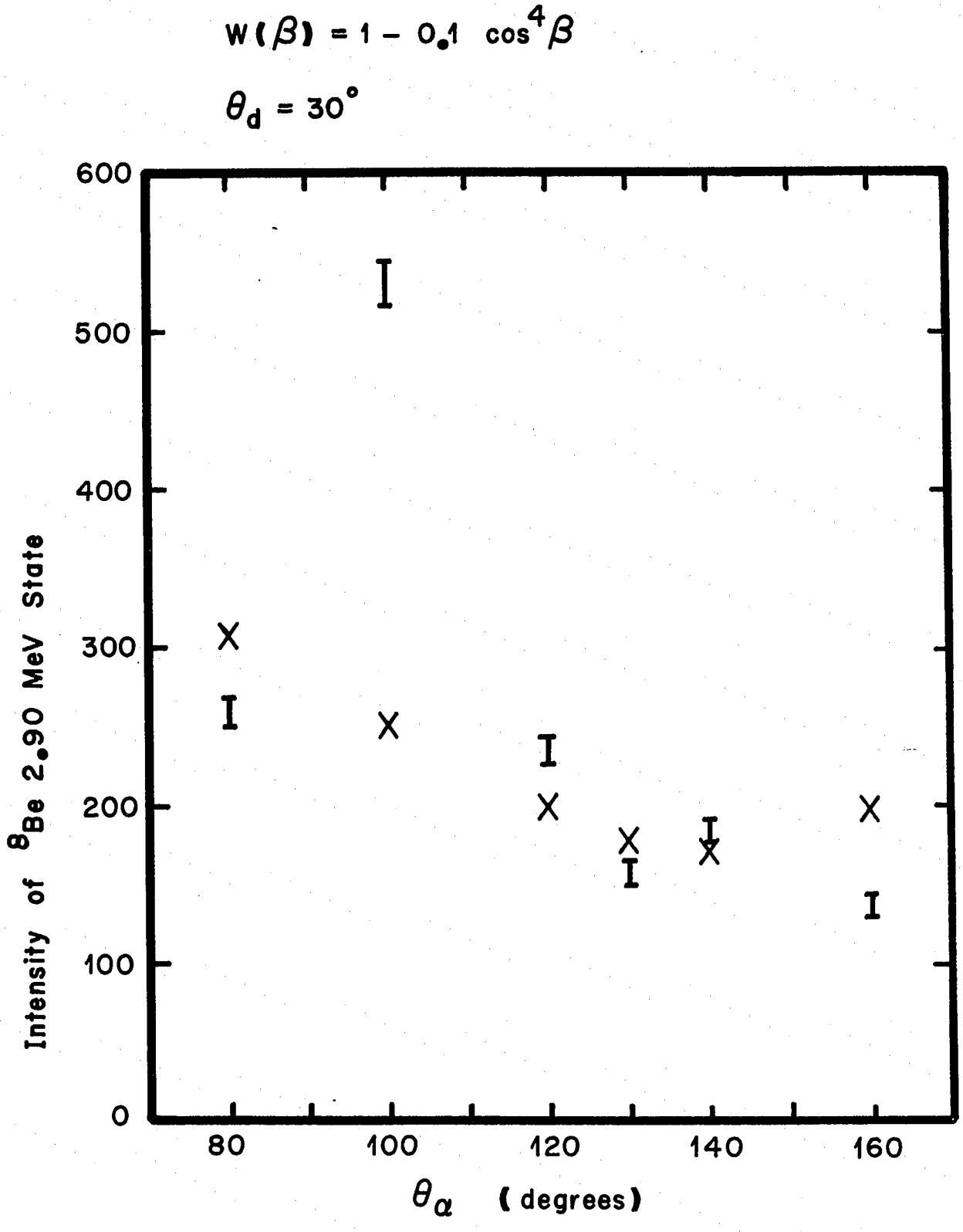
$W(\beta) = 1 - 0.1 \cos^4\beta$
$\theta_d = 30°$
600
500
400
300
200
100
0
Intensity of ^{8}Be 2.90 MeV State
80
100
120
140
160
θ_α (degrees)

in the recoil center of mass system. The complexity of these angular factors is the highest permitted by the quantum mechanical selection fules for the decay under the assumption of compound nucleus formation. The coefficients of the powers of cosβ were determined by a least square fit to the experimental data.

The fit for the angular dependence of the ^{6}Li 2.184 MeV state is relatively better than that for the ^{8}Be 2.90 MeV state, but neither is able to reproduce the data well. This is probably due to a significant contribution to the yield from a direct reaction first step, followed by a strong final state interaction, rather than the compound nucleus formation which is assumed by the theory. Excitation functions of the yield of deuterons and alpha particles in the region of 6 to 10 MeV bombarding energy show no strong resonance structure, indicating the absence of strong compound nucleus resonances. Further, Bleiden et al.[2] have observed the angular distributions of alpha particles from the ^{6}Li 2.184 MeV state and of deuterons from the ^{8}Be ground state at 9 MeV bombarding energy. The deuteron spectra show extremely strong forward peaking, indicating that the neutron pick-up mechanism is a strong channel for the ground state ^{8}Be yield. Unfortunately, the large width of the ^{8}Be 2.90 MeV state coupled with the deuteron continuum from the

three-body reaction prohibits investigation of the angular distribution of the yield of deuterons from the 2.90 MeV state. The present results seem to indicate however, that a significant portion of this yield is via a neutron pick-up first step.

The angular fit for the ^{6}Li 2.184 MeV state is considerably better than that for the ^{8}Be 2.90 MeV state. A triton pick-up first mechanism would be necessary for a single step direct reaction to contribute to this yield. One would expect the triton pick-up to be less strong than a single nucleon pick-up mechanism, since there is little evidence for a significant (t + ^{6}Li) cluster in the ^{9}Be target nucleus.

The conclusion that a direct-reaction competing mechanism contributes to the strong angular dependence of the ^{8}Be 2.90 MeV state yield is further reinforced by the results of Taylor[25]. He has used the same formalism (including the same computer program) to fit the angular dependence of the ^{8}Be 2.90 MeV state from the ^{9}Be + ^{3}He $\rightarrow 3\alpha$ reaction, where compound nucleus formation should be more probable. He achieves remarkably good fits to the experimental data.

Another possible explanation for the poor quality of the fits to the angular dependence of the yield is that interference effects exhibit a strong angular-dependence.

Bronson et al.[12] have observed such interference effects in the $^{11}B + p \rightarrow 3\alpha$ reaction. No attempt has been made to include these effects in the theory presented here, but efforts to include these effects are currently underway.

It is evident that three-body reactions present challenging problems both from experimental and theoretical standpoints. Many nuclei possess particle-unstable states whose properties can only be studied in detail by an experiment which completely determines the kinematics of the final state of the decaying many-body system. Considerable progress has been made in understanding these processes in the last few years. The present results, coupled with those of Simpson[14], Jackson[20], and Aldridge[26], indicate that the density of states formalism is quite successful in predicting the shape of the final state interaction yield. Further, when the reaction proceeds through a strong compound nucleus resonance, the angular dependence of the yield can be treated using the theory of Goldfarb[34]. However, competing mechanisms can produce enhancement of yield, and the theoretical treatment of the yield due to these competing mechanisms deserves further study.

APPENDIX A

Kinematics for Three-Body Decay

It is desired to calculate the loci of all possible values of T_2 (the kinetic energy of the particle in detector 2 at laboratory angles θ_2, ϕ_2 to the incident beam) as a function of T_1 (the kinetic energy of the particle in detector 1 at angles θ_1, ϕ_1). The momentum and energy conservation requirements may be written as follows:

$$P_o = \sum_{i=1}^{3} P_i \cos \theta_i \tag{1}$$

$$0 = \sum_{i=1}^{3} P_i \sin \theta_i \sin \phi_i \tag{2}$$

$$0 = \sum_{i=1}^{3} P_i \sin \theta_i \cos \phi_i \tag{3}$$

$$\frac{P_o^2}{2m_o} + Q = \frac{1}{2} \sum_{i=1}^{3} \frac{P_i^2}{m_i} \tag{4}$$

where the i subscripts refer to the three particles in the final state, and the zero subscripts refer to the beam particle. We can eliminate ϕ_3 using equations (2) and (3) yielding:

$$P_3^2 \sin^2\theta_3 = [P_1 \sin \theta_1 \sin \phi_1 + P_2 \sin \theta_2 \sin \phi_2]^2 + [P_1 \sin \theta_1 \cos \phi_1 + P_2 \sin \theta_2 \cos \phi_2]^2 \tag{5}$$

Combining equations (5) and (1) and substituting the result into (4) yields:

$$P_2^2\left[\frac{1}{2m_2}+\frac{1}{2m_3}\right]+\frac{P_2}{m_3}\left[P_1\cos\theta_1\cos\theta_2+P_1\sin\theta_1\sin\theta_2\cos(\phi_1-\phi_2)-P_o\cos\theta_2\right]$$

$$+P_1^2\left(\frac{1}{2m_1}+\frac{1}{2m_3}\right)+P_o^2\left(\frac{1}{2m_3}-\frac{1}{2m_o}\right)-\frac{1}{m_3}P_oP_1\cos\theta_1-Q=0$$

We may now calculate P_2 as a function of P_1 for fixed angles θ_1, θ_2, ϕ_1, ϕ_2:

$$P_2=\frac{-B\pm\sqrt{B^2-4AC}}{2A}$$

where

$$A=\left[\frac{1}{2m_3}+\frac{1}{2m_2}\right]$$

$$B=\frac{1}{m_3}\left[P_1\cos\theta_1\cos\theta_2+P_1\sin\theta_1\sin\theta_2\cos(\phi_1-\phi_2)-P_o\cos\theta_2\right]$$

$$C=\left[P_o^2\left(\frac{1}{2m_3}-\frac{1}{2m_o}\right)+P_1^2\left(\frac{1}{2m_1}+\frac{1}{2m_3}\right)-\frac{1}{m_3}P_oP_1\cos\theta_1-Q\right]$$

Thus the solution is double valued, and solutions will be referred to as P_2^+ and P_2^-, corresponding to the two branches of the quadratic. From this relation, T_2 may be easily calculated as a function of T_1, but with the restriction that only positive momenta represent particles traveling toward the detectors, and hence only when both P_1 and P_2 are positive will the solution correspond to a detectable portion of the locus.

APPENDIX B

Kinematics for Sequential Decay

The kinematic relations of Appendix A are, of course, valid irrespective of the mechanism of the reaction. However, it is possible to derive the internal energies of the various two-particle systems in the case in which the reaction proceeds sequentially via a pair of two-body disintegrations.

Consider the reaction proceeding in two steps:

a) $A + B \rightarrow i + (jk)$

b) $i + (jk) \rightarrow i + j + k$

where we may allow any possible permutation of the indices i, j, and k. Applying the conservation of momentum and the conservation of energy we obtain:

$$T_o + Q = T_i + T_{jk} + E_{jk} \tag{1}$$

$$P_o = P_i \cos\theta_i + P_{jk} \cos\theta_{jk} \tag{2}$$

$$0 = P_i \sin\theta_i \sin\phi_i + P_{jk} \sin\theta_{jk} \sin\phi_{jk} \tag{3}$$

$$0 = P_i \sin\theta_i \cos\phi_i + P_{jk} \sin\theta_{jk} \cos\phi_{jk} \tag{4}$$

where T_{jk} is the kinetic energy of the cluster (jk) and E_{jk} is its internal energy. Since the two-body kinematics restrict the first breakup to a plane,

$$\phi_i = \phi_{jk} + \pi$$

Using this relation, both ϕ_i and ϕ_{jk} may be eliminated between equations (3) and (4):

$$P_{jk}^2 \sin^2\theta_{jk} = P_i^2 \sin^2\theta_i$$

We may also eliminate θ_{jk} using (2) and (3):

$$P_{jk}^2 = P_i^2 \sin^2\theta_i + (P_o - P_i\cos\theta_i)^2$$

$$P_{jk}^2 = P_o^2 + P_i^2 - 2P_oP_i\cos\theta_i$$

Thus

$$T_{jk} = \frac{1}{2m_{jk}} (P_o^2 + P_i^2 - 2P_oP_i\cos\theta_i)$$

and using equation (1) we obtain the result:

$$E_{jk} = T_o + Q - T_i - \frac{1}{2m_{jk}} (P_o^2 + P_i^2 - 2P_oP_i\cos\theta_i)$$

If particle 1 (the particle in detector 1) is the first emitted particle, then the internal energy in the recoil (2-3) system is:

$$E_{23} = T_o + Q - T_1 - \frac{1}{2m_{23}} (P_o^2 + P_1^2 - 2P_oP_1\cos\theta_1)$$

Thus E_{23} is a single-valued function of T_1.

If particle 2 is the first emitted particle, then the energy in the recoil (1-3) system is:

$$E_{13} = T_o+Q - T_2 - \frac{1}{2m_{13}} (P_o^2 + P_2^2 - 2P_oP_2\cos\theta_2)$$

This is a single-valued function of T_2, but since T_2 is a double-valued function of T_1, E_{13} is also a double-valued function of T_1. The two solutions for E_{13} as a function of T_1 are given by

$$E_{13}^{\pm} = T_o+Q - T_2^{\pm} - \frac{1}{2m_{13}} (P_o^2 + (P_2^{\pm})^2 - 2P_oP_2^{\pm}\cos\theta_2)$$

Similarly, if particle 3 is the first emitted particle, the internal energy in the recoil (1-2) system is a double-valued function of T_1, and is given by:

$$E_{12}^{\pm} = T_o+Q - \frac{P_o^2}{2m_3} + \frac{P_o}{m_3} (P_1\cos\theta_1 + P_2^{\pm}\cos\theta_2)$$

$$- \frac{1}{2} \left(\frac{1}{m_3} + \frac{1}{m_{12}}\right)\Big\{P_1^2 + (P_2^{\pm})^2$$

$$+ 2P_1P_2^{\pm} [\cos\theta_1 \cos\theta_2 + \sin\theta_1 \sin\theta_2 \cos(\phi_1-\phi_2)]\Big\}$$

APPENDIX C

Density of States Calculations

Phillips, Griffy, and Biedenharn[19] suggest several different forms of the density of states functions. Fits to the ^{9}Be + p data were attempted with two of these:

I. $$\rho_{\ell}(E,a) = \frac{\mu}{\pi\hbar^2 k}\left[\frac{d}{dk}(\delta_{\ell}+\varphi_{\ell}) - \frac{1}{2}\left(\frac{1}{k} - \frac{2\frac{\partial A_{\ell}}{\partial k}}{A_{\ell}}\right)\sin 2(\delta_{\ell}+\phi_{\ell})\right.$$

$$\left. - \frac{1}{k}\left\{A_{\ell}\frac{\partial^2 A_{\ell}}{\partial r\,\partial k} - \frac{\partial A_{\ell}}{\partial r}\frac{\partial A_{\ell}}{\partial k}\sin^2(\delta_{\ell}+\phi_{\ell})\right\}\right] \quad \text{(renormalized form)}$$

II. $$\rho_{\ell}(E,a) = \frac{2\mu a}{\pi\hbar^2\gamma^2}\left[\frac{\sin^2(\delta_{\ell}+\phi_{\ell})}{P_{\ell}}\right] \qquad (\sin^2 \text{ form})$$

Here δ_{ℓ} and ϕ_{ℓ} are the nuclear and Coulomb phase shifts, $A_{\ell} = (F_{\ell}^2 + G_{\ell}^2)^{1/2}$, with F_{ℓ} and G_{ℓ} the regular and irregular Coulomb wave functions, and γ^2 is a constant. In the event the phase shift of the resonance is given by the Breit-Wigner single level formula $(\tan^{-1}\frac{\Gamma/2}{E_o - E})$ then γ^2 is the reduced width of the resonance.

The calculations for the alpha-alpha interaction were made using the alpha-alpha experimental phase shifts as summarized by Russell, Phillips, and Reich[27], based on their own measurements together with lower energy measurements of Cowie, Heydenburg, Temmer, and Little[28], and

higher energy measurements by Nilson and Jentschke. For the extremely narrow ^{8}Be ground state resonance at 94 keV, a Breit-Wigner form was assumed for the phase shift using a center of mass width of 6.8 eV as quoted by Lauritsen and Ajzenberg-Selove[29], and the effective radius of 7.5 F calculated by Beckner, Jones, and Phillips[30]. The density of states factors were calculated in steps of 0.1 eV across this ground state resonance.

The extremely narrow width of this resonance presented some calculational problems. The fitting program must take energy steps which are small compared to the rate of change of the density of states factors in order to avoid computational errors. However, to take energy steps small compared to the rate of change of the density of states across this narrow resonance would require an inordinate amount of computer time. Therefore, the density of states function was integrated over the resonance, and replaced by a gaussian curve of width 800 eV, whose integral was the same as that of the "real" resonance. This width still appeared extremely narrow to the fitting program, but the computation time was reduced to manageable proportions. The calculation of the density of states functions for the 2.90 MeV state in ^{8}Be was carried out in a straightforward manner using the experimental phase shifts previously mentioned, and an

effective radius of 3.5 F as calculated by Beckner *et al.*[30]

The deuteron-alpha density of states functions were calculated using the experimental phase shifts of Galonsky and McEllistrem[31], based on the work of Galonsky, Douglas, Haeberli, McEllistrem, and Richards[32]. A Breit-Wigner form for the 2.184 MeV resonance was assumed, using a width of 25 keV and an effective radius of 3.5 F as given by Galonsky *et al.*[31]

APPENDIX D

Angular Correlation Factors

The problem of calculating the angular dependence of successive radiations by a quantum mechanical system has been considered by a number of authors. (See references 33 through 36.) As Biedenharn[33] points out, the difficulty lies in the fact that a system which sequentially radiates to a final state of three or more particles has no natural axis of quantization, due to the effects of recoil, so that it is difficult to invoke symmetry relations to simplify the problem.

Goldfarb[34] and Devons and Goldfarb[35] have treated the problem by making use of angular momentum and parity properties of nuclear systems, and their symmetry properties under spatial rotation and time-reversal. A summary of these results will be given here, as they relate to the three-body sequential decay of an excited nucleus.

The notation is as follows: A projectile with spin $\vec{\sigma}_1$ bombards a target with spin $\vec{\sigma}_2$ with relative angular momentum $\vec{\ell}_1$, to form a compound nucleus with total angular momentum $\vec{b}$. The spins of the beam and target are coupled to form a channel spin $\vec{a} = \vec{\sigma}_1 + \vec{\sigma}_2$. The compound system decays by emitting a particle of spin $\vec{s}_1$ and relative angular

momentum $\vec{\ell}_2$, leaving a recoiling metastable nucleus with spin $\vec{c}$. The channel spin of this intermediate system is denoted by $\vec{j} = \vec{s}_1 + \vec{c}$. Subsequently, the recoil system breaks up into two particles of spin $\vec{s}_2$ and $\vec{s}_3$ respectively, and with relative angular momentum $\vec{\ell}_3$. $\vec{m} = \vec{s}_2 + \vec{s}_3$. If the beam axis is chosen as the axis of quantization, the angular correlation of the successive radiations as derived by Devons and Goldfarb[35] is:

$$W \sim \Sigma (-1)^{a-b'+s_1+\ell_2'-j-c-c'+m} \hat{b}^2 \hat{b}'^2 \hat{\ell}_1 \hat{\ell}_1' \hat{\ell}_2 \hat{\ell}_2' \hat{\ell}_3 \hat{\ell}_3' \hat{j}\, \hat{j}'\, \hat{c}\, \hat{c}'$$

$$(\ell_1 0\, \ell_1 0 | k_b 0)\, (\ell_2 0\, \ell_2 0 | k_2 0)\, (\ell_3 0\, \ell_3 0 | k_j 0)$$

$$W(j\ j'\ c\ c' | k_j s_1)\ W(c\ c'\ \ell_3\ \ell_3' | k_j m)\ \ W(\ell_1 \ell_1'\ b\ b' | k_b\ a)$$

$$\begin{Bmatrix} \ell_2 & j & b \\ \ell_2' & j' & b' \\ k_2 & k_j & k_b \end{Bmatrix} \sum_{\eta} (k_2\, \eta\, k_j - \eta\, |\, k_b 0) Y^{\eta}_{k_2}(\theta_1', \phi_1') Y^{-\eta}_{k_j}(\theta_2'', \phi_2'')$$

where the quantities $\hat{k}$ represent $(2k+1)^{1/2}$, and the primed numbers represent the values of the quantum numbers after the emission of any unobserved radiation. For the case of three-body decay under the assumptions given, the primed quantum numbers and the unprimed quantum numbers are equal.

The angles (θ_1', ϕ_1') are expressed in the system center of mass system, while (θ_2'', ϕ_2'') are in the recoil center of mass system.

REFERENCES

1. G. C. Phillips and T. A. Tombrello, Nuclear Physics 19 (1960) 555;
T. A. Tombrello and G. C. Phillips, Nuclear Physics 20 (1960) 648.

2. H. R. Blieden, G. M. Temmer, and K. L. Warsh, Nuclear Physics 49 (1963) 209.

3. S. Morita, T. Tohei, T. Nakagawa, T. Hasegawa, H. Ueno, and H. Chu-Chung, Nuclear Physics 66 (1965) 17.

4. R. Ishiwari, Bull. Inst. of Chemical Research, Kyoto Univ. (Japan) 39 (1961) 287.

5. J. P. Laugier, C. Lemeille, L. Marguoz, and N. Saunier, Nuclear Physics 88 (1966) 411.

6. E. H. Beckner, C. M. Jones, and G. C. Phillips, Phys. Rev. 123 (1961) 255.

7. H. J. Hay, E. F. Scarr, D. J. Sullivan, and P. B. Treacy, Australian National Univ., ANU-P/371 (1962).

8. S. T. Emerson, W. Dwain Simpson, J. C. Legg, and G. C. Phillips, Nuc. Inst. and Meth. 52 (1967) 229.

9. A.C.L. Barnard, R. Keyes, J. Buchanan, T. A. Rabson, and G. C. Phillips, Bull. Am. Phys. Soc. 9 (1964) 488;

A.C.L. Barnard, R. Keyes, J. Buchanan, T. A. Rabson and G. C. Phillips, Nuc. Inst. and Methods 31 (1964) 147.

10. G. C. Phillips, Rev. Mod. Phys. 37, No. 3 (1965) 409.

11. W. D. Simpson, J. D. Bronson, W. R. Jackson, and G. C. Phillips, Rev. Mod. Phys. 37, No. 3 (1965) 523.

12. J. D. Bronson, W. D. Simpson, W. R. Jackson, and G. C. Phillips, Nuc. Phys. 68, No. 2 (1965) 241;
J. D. Bronson, Ph.D. Thesis, Rice University (1964) (unpublished).

13. Y. S. Chen, S. T. Emerson, W. R. Jackson, W. D. Simpson, and G. C. Phillips, Nuc. Phys. A106 (1968) 1;
Y. S. Chen, M.A. Thesis, Rice University (1967) (unpublished).

14. W. D. Simpson, W. R. Jackson, and G. C. Phillips, Nuc. Phys. A103 (1967) 97;
W. D. Simpson, Ph.D. Thesis, Rice University (1965) (unpublished).

15. V. Valkovic, W. R. Jackson, Y. S. Chen, S. T. Emerson, and G. C. Phillips, Nuc. Phys. A96 (1967) 241.

16. V. Valkovic, C. Joseph, S. T. Emerson, and G. C. Phillips, Nuc. Phys. A106 (1968) 138.

17. K. M. Watson, Phys. Rev. 88 (1952) 1163.

18. A. B. Migdal, ZhETF(USSR) 28 (1955) 3.

19. G. C. Phillips, T. A. Griffy, and L. C. Biedenharn, Nuc. Phys. 21 (1960) 327.

20. W. R. Jackson, Ph.D. Thesis, Rice University (1967) (unpublished).

21. A. Niiler, C. Joseph, V. Valkovic, and G. C. Phillips, Bull. Am. Phys. Soc. 12 (1967) 1174.

22. G. C. Phillips, V. Valkovic, I. M. Duck, and W. D. Simpson, Bull. Am. Phys. Soc. 11 (1966) 751.

23. T. H. Berlin and G. E. Owen, Nuc. Phys. 5 (1958) 669.

24. Cao X. Chuan, J. Phys. Radium 23 (1962) 78.

25. M. C. Taylor, Ph.D. Thesis, Rice University (1968) (unpublished).

26. J. P. Aldridge, Ph.D. Thesis, Rice University (1965) (unpublished).

27. J. L. Russell, Jr., G. C. Phillips, and C. W. Reich, Phys. Rev. 104 (1956) 135.

28. Cowie, Heydenburg, Temmer, and Little, Phys. Rev. 86 (1952) 593.

29. T. Lauritsen and F. Ajzenberg-Selove, Nucl. Phys. 78 (1966) 1.

30. E. H. Beckner, C. M. Jones, and G. C. Phillips, Phys. Rev. 123 (1961) 255.

31. A. Galonsky and M. T. McEllistrem, Phys. Rev. 98 (1955) 590.

32. A. Galonsky, R. A. Douglas, W. Haeberli, M. T. McEllistrem, and H. T. Richards, Phys. Rev. 98 (1955) 586.

33. L. C. Biedenharn, "Angular Correlations," Nuclear Spectroscopy, Part B, ed. by F. Ajzenberg-Selove (Academic Press, New York, 1960).

34. L.J.B. Goldfarb, "Angular Correlations and Polarization," Nuclear Reactions, Vol. 1, ed. by P. M. Endt and M. Demeur (North Holland Publishing Co., Amsterdam, 1959).

35. S. Devons and L.J.B. Goldfarb, "Angular Correlations," Handbuch der Physik, Vol. 42, ed. by S. Flügge (Springer Verlag, Berlin, 1957).

36. F. Coester and J. M. Jauch, Helv. Phys. Acta, 26 (1953) 3.

ACKNOWLEDGEMENTS

The author wishes to express his deep appreciation to Professor G. C. Phillips for suggesting the project, for his many helpful suggestions, and for his encouragement. He is deeply indebted to Drs. W. D. Simpson and W. R. Jackson, Jr. for their invaluable help in all phases of the project. Professor J. C. Legg, and Dr. B. S. Bhakar contributed through many long and productive discussions. He is grateful to Drs. A. Niiler, V. Valkovic, C. Joseph, and M. C. Taylor for many hours of assistance in data collection, and other valuable contributions. Miss Karen Edwards' tireless help in data reduction is much appreciated, as is Miss Sandra Harrison's valuable help in constructing the assembler language data edit programs. Mr. James Buchanan contributed to the solution of many technical problems. Mr. Arthur S. Wilson's talented assistance in the graphic presentation of the data is gratefully acknowledged. Many others in the Rice University Physics Department and the T. W. Bonner Nuclear Laboratories have made valuable contributions. The author wishes to thank Rice University and the U. S. Atomic Energy Commission for financial assistance through the term of his graduate studies. Last he wishes to thank Mom and Dad, whose unfailing encouragement and patient guidance have made the entire effort possible.